HHS Public Access

Author manuscript

Nature. Author manuscript; available in PMC 2023 April 01.

Published in final edited form as:

Nature. 2022 October ; 610(7933): 744–751. doi:10.1038/s41586-022-05141-x.

ILC3s select microbiota-specific regulatory T cells to establish tolerance in the gut

Mengze Lyu[1,2,3,12], **Hiroaki Suzuki**[1,2,3,11,12], **Lan Kang**[1,2,3], **Fabrina Gaspal**[4], **Wenqing Zhou**[1,2,3], **Jeremy Goc**[1,2,3], **Lei Zhou**[1,2,3], **Jordan Zhou**[1,2,3], **Wen Zhang**[1,2,3], **JRI Live Cell Bank**[1], **Zeli Shen**[5], **James G. Fox**[5], **Robbyn E. Sockolow**[6], **Terri M. Laufer**[7,8], **Yong Fan**[9], **Gerard Eberl**[10], **David R. Withers**[4], **Gregory F. Sonnenberg**[1,2,3,*]

[1]Joan and Sanford I. Weill Department of Medicine, Division of Gastroenterology & Hepatology, Weill Cornell Medicine, Cornell University, New York, NY, USA

[2]Department of Microbiology and Immunology, Weill Cornell Medicine, Cornell University, New York, NY, USA

[3]Jill Roberts Institute for Research in Inflammatory Bowel Disease, Weill Cornell Medicine, Cornell University, New York, NY, USA

[4]Institute of Immunology and Immunotherapy, College of Medical and Dental Sciences, University of Birmingham, Birmingham, UK

[5]Division of Comparative Medicine, Massachusetts Institute of Technology, Cambridge, MA, USA

[6]Department of Pediatrics, Division of Gastroenterology, Hepatology, and Nutrition, Weill Cornell Medicine, Cornell University, New York, NY, USA

[7]Perelman School of Medicine, University of Pennsylvania, Philadelphia, PA, USA

[8]Philadelphia Veterans Affairs Medical Center, Philadelphia, PA, USA

[9]Institute of Cellular Therapeutics, Allegheny Health Network, Pittsburgh, PA, USA

[10]Microenvironment and Immunity Unit, Institut Pasteur, Paris, France

[11]Present address: EA Pharma, Kanagawa, Japan

[12]These authors contributed equally to this manuscript

Abstract

Microbial colonization of the mammalian intestine elicits inflammatory or tolerogenic T cell responses, but the mechanisms controlling these distinct outcomes remain poorly understood and accumulating evidence indicates that aberrant immunity to intestinal microbiota is causally

*Correspondence and requests for materials should be addressed to gfsonnenberg@med.cornell.edu.

H.S. is currently employed by EA Pharma Co., Ltd. Kanagawa, Japan.

Author contributions

M.L., H.S. and G.F.S. conceived the project. M.L. performed most experiments and analysed the data. H.S., L.K., F.G., J.G., W. Zhou, L.Z., W. Zhang and J.Z. helped with experiments and data analyses. J.G.F., Z.S., Y.F., T.M.L., G.E. and D.R.W. provided essential tools, scientific advice and expertise. R.E.S. and JRI Live Cell Bank contributed to clinical sample acquisition and processing. M.L. and G.F.S. wrote the manuscript, with input from all authors.

The authors declare no other competing interests.

associated with infectious, inflammatory, and malignant diseases[1–8]. Here, we define a critical pathway controlling the fate of inflammatory versus tolerogenic T cells that respond to the microbiota and express the transcription factor RORγt. We profiled all RORγt$^+$ immune cells at single cell resolution from the intestine-draining lymph nodes of mice and reveal a dominant presence of regulatory T cells (Tregs) and lymphoid tissue inducer-like group 3 innate lymphoid cells (ILC3s), which co-localize at interfollicular regions. These ILC3s are distinct from extrathymic Aire-expressing cells, abundantly express major histocompatibility complex class II, and are necessary and sufficient to promote microbiota specific RORγt$^+$ Tregs and prevent their expansion as inflammatory T helper (Th)17 cells. This occurs through ILC3-mediated antigen-presentation, αv integrin, and competition for interleukin-2. Finally, single-cell analyses suggest that ILC3 and RORγt$^+$ Treg interactions are impaired in inflammatory bowel disease. Our results define a paradigm whereby ILC3s select for antigen specific RORγt$^+$ Tregs, and against Th17 cells, to establish immune tolerance to the microbiota and intestinal health.

The mammalian gastrointestinal (GI) tract is continuously colonized with microbiota, opportunistic microbes, or pathogens, which induce robust responses that are often dominated by immune cells expressing the lineage-specifying transcription factor RORγt[1–17]. Depending on the adopted fate, these RORγt$^+$ cells orchestrate immunity, inflammation or tolerance in the intestine[9–17] and substantial alterations in numbers or function of RORγt$^+$ immune cells occur in multiple chronic human diseases, including inflammatory bowel disease (IBD), human immunodeficiency virus infection and cancer[1–18]. Despite these advances, the full spectrum of cellular heterogeneity among RORγt$^+$ immune cells, the potential for functional interactions among subsets, and the pathways that are necessary to establish immune tolerance in the context of a complex microbiota remain poorly defined.

Defining all RORγt$^+$ cells in the mLN

RORγt$^+$ cell types include T helper (Th)17 cells, regulatory T cells (Tregs), γδ T cells, and group 3 innate lymphoid cells (ILC3s), as well as a few other potential cell types that were only recently characterized[17,19,20]. To uncover the full spectrum of cellular heterogeneity and examine for pathways impacting tolerance or inflammation in response to microbes, we performed single-cell RNA-sequencing (scRNA-seq) on all RORγt$^+$ cells from the intestine-draining mesenteric lymph nodes (mLN) of healthy RORγt-eGFP reporter mice (Extended Data Fig. 1a). T cells are dominant in this tissue, and we therefore sequenced an equal ratio of T cells (GFP$^+$TCRβ$^+$) to non-T cells (GFP$^+$TCRβ$^-$) to increase the resolution of rare RORγt$^+$ cell types. This revealed 14 distinctive clusters, each of which was annotated based on select marker genes and visualized by uniform manifold approximation and projection (UMAP) (Fig. 1a). Two clusters were excluded from future analyses, including cluster 8 that was identified as a doublet population (Extended Data Fig. 1b) and cluster 7 that was identified as B cells but could not be verified by RORγt reporter or fate mapping approaches (Extended Data Fig. 1c, d), likely representing a contaminate. The remaining clusters exhibited expression of RORγt and could be divided into T cells versus non-T cells based on expression of *Cd3e* (Extended Data Fig. 1e, f). T cell subsets were dominated by RORγt$^+$ Tregs defined by expression of *Trac*, *Cd4* and *Foxp3* in cluster 0, 5 and

13, followed by Th17 cells expressing *Trac*, *Cd4* and *Il17a* in cluster 1, and γδ T cells expressing *Trdc* in clusters 4 and 9 (Fig. 1b, Extended Data Fig. 1g). Among the non-T cells, nearly all clusters were ILC3s, or ILC3-like cells, based on expression of *Id2* and *Il7r*, including a dominant population of lymphoid tissue inducer (LTi)-like ILC3s that express *Ccr6* and *Cd4* in cluster 2, T-bet$^+$ ILC3s that express *Ncr1* in clusters 3 and 12, and a minor population of group 2 innate lymphoid cell (ILC2)-like cells that express high *Gata3* and *Il17rb* in cluster 10 (Fig. 1c). Subsets of conventional type 2 dendritic cells (cDC2s) were suggested to express RORγt in the spleen[20], but in a recent report we were unable to identify this population in the intestine[21]. Further, we could not identify this population in our single cell analyses of the mLN and found minimal RORγt in cDC2s in this tissue as determined by flow cytometry on reporter or fate mapping mice (Extended Data Fig. 1c, d, h–k). Instead, the remaining two non-T cell clusters (cluster 6 and 11) were defined by expression of *Aire* (Fig. 1c), most closely resembling extrathymic Aire-expressing cells (eTACs) that several groups defined are RORγt$^+$, enriched in lymph nodes during early life developmental windows, and share transcriptional similarities with ILC3s, DCs and thymic epithelial cells[19,22].

Given this heterogeneity among innate RORγt$^+$ immune cells, we next sought to understand the phenotype and functions of ILC3s versus RORγt$^+$ eTACs. Differential analysis of LTi-like ILC3s (cluster 2) and the dominant RORγt$^+$ eTACs (cluster 6) revealed distinct gene signatures (Fig. 1d). Further validation revealed that LTi-like ILC3s are defined by high expression of CD127, CD25, CD122, LY6A (also known as SCA1) and CXCR6, while RORγt$^+$ eTACs are defined by high expression of SIGLECG, DPP4 and integrin α4β7 (Fig. 1e, Extended Data Fig. 2a–c). Importantly, LTi-like ILC3s express significantly higher levels of RORγt than eTACs (Fig. 1d, e, Extended Data Fig. 2c). We developed a novel gating strategy to isolate these cell types and confirmed that expression of *Aire* is exclusive to RORγt$^+$ eTACs and not observed in ILC3s (Fig. 1f, Extended Data Fig. 3a). These gating strategies do not rely on Aire and therefore include eTAC subsets that express low levels of this transcription factor. Notably, RORγt$^+$ eTACs did not exhibit expression of previously defined Aire-dependent tissue-specific antigens, but rather expressed several genes associated with a transient-amplifying Aire$^+$ thymic epithelial cell[23,24] (Supplementary Table 1). A previous study inferred that ILC3s have the potential to convert into RORγt$^+$ eTACs *in vitro* following RANK-RANKL stimulation[19], this provokes fundamental questions about the *in vivo* distinction of these two cell types. We determined that a majority of RORγt$^+$ eTACs fate-mapped positive for CD127-Cre, despite lacking CD127 staining, and exhibited limited fate-mapping for CD11c-Cre or Clec9a-Cre, which is comparable to LTi-like ILC3s (Fig. 1g, Extended Data Fig. 3a, b). In addition, RORγt$^+$ eTACs fate-mapped positive for Aire-Cre, and so do a minor proportion of LTi-like ILC3s in the mLN (Fig. 1h, Extended Data Fig. 3b) suggesting for the potential of interconversion among these cell types. Collectively, these data define the full spectrum of innate and adaptive immune cells that express the lineage-specifying transcription factor RORγt in the mLN of healthy mice, revealing a dominance of RORγt$^+$ Tregs and LTi-like ILC3s, as well as determining phenotypic distinctions between RORγt$^+$ eTACs and LTi-like ILC3s.

RORγt+ Tregs require MHCII+ ILC3s

We next sought to explore for functional interactions between innate and adaptive RORγt$^+$ cells in mLN by examining for their spatial proximity in the interfollicular zone, an area we previously found to contain a majority of ILC3s and other RORγt$^+$ T cells[25,26]. Indeed, ILC3s were rare in B cell follicles and T cell zones, but robustly present in interfollicular zones, which contrasts to more diffuse localization patterns of CD11c$^+$ cells (Extended Data Fig. 4). Strikingly we observed that CD3$^-$RORγt$^+$CD127$^+$ ILC3s were adjacent to CD3$^+$RORγt$^+$FoxP3$^+$ Tregs in the interfollicular zones, where a substantial portion of total RORγt$^+$ Tregs were associated with ILC3s (Fig. 2a, Extended Data Fig. 4). CD103$^+$ dendritic cells (DCs) have the potential to induce the differentiation of RORγt$^+$ Treg from naïve T cells[27–30], however both CD103$^+$ and CD103$^-$ DCs are redundant in promoting peripheral Treg differentiation[31], indicating other cell types regulate this process. Our previous work demonstrated LTi-like ILC3s limit microbiota-specific Th17 cells via major histocompatibility complex class II (MHCII) and a process termed “intestinal selection”[26,32]. Therefore, we next interrogated whether LTi-like ILC3s impact RORγt$^+$ Treg through MHCII and observed that LTi-like ILC3s abundantly express MHCII protein and transcripts in the mLN of healthy mice (Fig. 2b, Extended Data Fig. 5a). Further, MHCII$^{\Delta ILC3}$ mice that were generated by crossing *H2-Ab1*$^{fl/fl}$ mice with *Rorc*^{Cre} mice[32] exhibited a highly selective deletion of MHCII in ILC3s relative to other immune cells in the draining mLN and large intestine (Fig. 2c, Extended Data Fig. 3c). In mice lacking ILC3-specific MHCII, we identified a striking and significant reduction in the frequency of RORγt$^+$ Tregs in both mLN and large intestine relative to littermate control mice (Fig. 2d–h). We previously reported that MHCII$^{\Delta ILC3}$ mice exhibit spontaneous intestinal inflammation[32], and consistent with this we observe significantly increased total cell numbers of CD4$^+$ T cells and Th17 cells within the large intestine, with a significant decrease in numbers of RORγt$^+$ Tregs (Extended Data Fig. 5b–e). These results were specific to MHCII$^+$ LTi-like ILC3s, as deletion of MHCII by targeting T cells with CD4-cre or ILC2s with IL-5-cre, and deletion of RORγt by targeting T-bet$^+$ ILC3s with Ncr1-cre, did not impact the frequency of RORγt$^+$ Tregs or other CD4$^+$ T cell subsets in the large intestine (Extended Data Fig. 5f–k). RORγt$^+$ eTACs also express MHCII as previously shown[19], but *Rorc*^{Cre} only modestly targeted deletion of MHCII on RORγt$^+$ eTACs and this is likely due to their significantly lower expression of RORγt relative to ILC3s (Fig. 1d, e, Fig. 2c, Extended Data Fig. 5a). Further, targeting of RORγt$^+$ eTACs indicate a redundant role for this population in modulating RORγt$^+$ Tregs as comparable frequencies were present in *Rorc*^{Cre}*Aire*$^{fl/fl}$ mice, *Aire*^{Cre}*Rorc*$^{fl/fl}$ mice, and *Aire*^{Cre}*H2-Ab1*$^{fl/fl}$ mice relative to littermate controls (Fig. 2i–k, Extended Data Fig. 5l–o). LTi-like ILC3s were also comparable in *Aire*^{Cre}*Rorc*$^{fl/fl}$ mice relative to littermates (Extended Data Fig. 5n), indicating that RORγt$^+$ eTACs are redundant to maintain this population in homeostasis. RORγt$^+$ Tregs were present at comparable frequencies in *Clec9a*^{Cre}*H2-Ab1*$^{fl/fl}$ mice relative to literate controls, indicating a redundancy of cDCs (Fig. 2l, Extended Data Fig. 5p). Finally, an *ex vivo* co-culture system revealed that RORγt$^+$ Tregs increased in frequency and cell number when in the presence of LTi-like ILC3s, as well as exhibited reduced Bim, increased Nur77 staining and minor changes in cell death at this time point (Extended Data Fig. 6a–e), indicating that LTi-like ILC3s are sufficient to support RORγt$^+$ Tregs.

ILC3s select microbiota specific Tregs

RORγt$^+$ T cells develop in response to antigens derived from microbiota that colonize the mammalian intestine. For example, studies demonstrated that segmented filamentous bacteria (SFB) promote antigen-specific Th17 cells[33], while *Helicobacter hepaticus* (*H. hepaticus*) promote antigen-specific RORγt$^+$ Tregs[34] in the intestine of wild-type mice. Therefore, we next examined whether MHCII$^+$ ILC3s regulate both Th17 cells and RORγt$^+$ Tregs that recognize distinct microbiota-derived antigens in the intestine. To accomplish this, we transferred congenic-marked naïve T cells from SFB-specific TCR transgenic mice and *H. hepaticus*-specific TCR transgenic mice into recipients that were colonized with both microbes (Extended Data Fig. 7a). Two weeks post-transfer, we analyzed the donor T cell populations and observed comparable upregulation of CD44 in recipient littermate controls and MHCII$^{\Delta ILC3}$ mice (Extended Data Fig. 7b, c). This indicates that ILC3s are not required to prime antigen-specific T cells and is consistent with the absence of ILC3s from T cell zones of lymph nodes (Extended Data Fig. 4)[26]. SFB-specific T cells differentiated into Th17 cells in littermate control mice and a significantly expanded Th17 cell population was observed in mice lacking ILC3-specific MHCII (Fig. 3a, b). The impairment of RORγt$^+$ Tregs is insufficient to drive expansion of effector Th17 cells, such as the SFB-specific T cell populations, as comparable intestinal Th17 cells were observed in *Foxp3*^{Cre}*Rorc*$^{fl/fl}$ mice (Extended Data Fig. 7d). In contrast, we observed that intestinal *H. hepaticus*-specific T cells failed to express FoxP3 in mice lacking ILC3-specific MHCII, and rather adopted a RORγt$^+$ Th17 cell phenotype relative to those transferred to littermate controls (Fig. 3c, d, Extended Data Fig. 3d). In the absence of ILC3-specific MHCII, the *H. hepaticus*-specific T cell upregulated T-bet and co-produced significantly more IFNγ and IL-17A (Fig. 3e–h). Importantly, we observed a significant impairment in the differentiation of *H. hepaticus*-specific RORγt$^+$ Tregs when ILC3s were targeted in *Il22*^{Cre}*H2-Ab1*$^{fl/fl}$ mice, and in this context, there was a partial but selective deletion of MHCII on ILC3s in the mLN and no targeting of MHCII$^+$ eTACs (Extended Data Fig. 7e–g). These data demonstrate that ILC3-specific MHCII is necessary to both limit the expansion of microbiota specific Th17 cells as we previously described[26,32], while simultaneously enforcing microbiota specific RORγt$^+$ Treg populations and preventing their ability to expand as proinflammatory Th17 cells.

We also interrogated whether MHCII$^+$ ILC3s are sufficient to promote microbiota specific RORγt$^+$ Tregs by utilizing mice in which MHCII expression is restricted to only ILC3s[26]. Revisiting *H2-Ab1*-STOP$^{fl/fl}$ mice (MHCII^{neg}) and those crossed to *Rorc*^{Cre} mice (MHCII^{ILC3+}) revealed a robust expression of MHCII restricted only to ILC3s, but not on cDCs in the mLN and large intestine, as well as a lack of MHCII on RORγt$^+$ eTACs in the mLN that is likely due to the limited expression of *Rorc* (Fig. 3i, j, Extended Data Fig. 7h). We next transferred congenic-marked naïve T cells from *H. hepaticus*-specific TCR transgenic mice into recipients that were colonized with *H. hepaticus* as above. Two weeks post-transfer, we analyzed the donor T cell populations and observed comparable upregulation of CD44 and downregulation of CD62L in recipient MHCII^{neg} and MHCII^{ILC3+} mice (Extended Data Fig. 7i). This suggest that even with the lack of MHCII in this MHCII^{neg} mouse model, there remains some endogenous priming of naïve

H. hepaticus-specific T cells. However, when analyzing the fate of these T cells, it was clear that MHCII expression on ILC3s is sufficient for *H. hepaticus*-specific T cells to efficiently adopt a RORγt$^+$ Treg fate in both the mLN and large intestine (Fig. 3k, l). These results collectively demonstrate that MHCII$^+$ ILC3s are necessary and sufficient to critically select for the fates of RORγt$^+$ T cells by simultaneously promoting Tregs and limiting Th17 cells of distinct antigen-specificities.

ILC3s support RORγt$^+$ Tregs via Itgav

We next mechanistically examined how MHCII$^+$ ILC3s promote RORγt$^+$ Tregs. Analyses of the remaining RORγt$^+$ Treg population in MHCII$^{\Delta ILC3}$ mice revealed a significant increase in Bim but comparable levels of Ki-67 (Extended Data Fig. 7j, k), suggesting there are alterations in cell survival but not proliferation. Defined receptor-ligand analyses in our scRNA-seq data demonstrated that MHCII$^+$ LTi-like ILC3s may interact with RORγt$^+$ Tregs through cytokine-cytokine receptors or integrin Itgav-mediated processing of transforming growth factor (TGF)-β (Fig. 4a). Subsets of ILC3s produce IL-2 to support Treg homeostasis in the small intestine[35], but ablation of IL-2 in all RORγt$^+$ cells did not impact the presence of RORγt$^+$ Tregs in the large intestine (Extended Data Fig. 7l). We also previously defined that ILC3-mediated sequestration of IL-2 mechanistically contributed to their ability to limit effector T cell responses[26], and analyses of IL-2 binding and CD25 levels revealed that RORγt$^+$ Tregs were significantly more efficient at competing for this survival cytokine over naïve or effector T cell populations (Extended Data Fig. 7m). This indicates a contribution of IL-2 competition among innate and adaptive RORγt$^+$ cell types. We next explored integrins that mediate processing of TGF-β, as prior reports identified a critical role of DC-mediated processing of TGF-β by integrin αvβ8 in the support of Tregs[36–38] and that loss of TGFβR on Tregs results in upregulation of Bim[39]. We explored what β-integrins pair with Itgav on ILC3s and found moderate levels of *Itgb1*, *Itgb3*, and *Itgb5* expression on ILC3s in the mLN and large intestine, but a lack of *Itgb6* and *Itgb8* (Fig. 4a, b). Utilizing our *ex vivo* co-culture system, we found that blockade of Itgav or Itgb3 significantly abrogated ILC3-mediated support of RORγt$^+$ Tregs and suppression of Th17 cells (Fig. 4c). This indicates that ILC3s interact with RORγt$^+$ Tregs in part through αvβ3 integrin, which has previously been linked to processing of latent TGF-β and several other extracellular ligands[40]. Consistent with this, we found that ILC3s in the mLN and intestine stained highly for integrin αv (Itgav), and that this could be successfully deleted by crossing *Itgav*$^{fl/fl}$ mice with *Rorc*^{Cre} mice, while Itgav remained intact on RORγt$^+$ eTACs in these mice likely due to the limited expression of *Rorc* (Fig. 4d, Extended Data Fig. 8a). Consistent with the role we identified for MHCII$^+$ ILC3s, we observed a significant reduction in the frequency of RORγt$^+$ Tregs and a significant increase in the frequency of Th17 cells in both the mLN and large intestine of *Rorc*^{Cre}*Itgav*$^{fl/fl}$ mice relative to littermate control mice (Fig. 4e). Further, comparable frequencies of RORγt$^+$ Tregs were present in mLN of *Cd4*^{Cre}*Itgav*$^{fl/fl}$ mice relative to littermate control mice, suggesting Itgav on ILC3s, but not on CD4$^+$ T cells, was involved in promoting RORγt$^+$ Tregs (Extended Data Fig. 8b–e). In addition, *H. hepaticus*-specific T cells failed to robustly differentiate into RORγt$^+$ Tregs, and rather expanded as Th17 cells in both the mLN and large intestine of *Rorc*^{Cre}*Itgav*$^{fl/fl}$ mice relative to littermate controls (Fig. 4f, Extended Data Fig. 8f). Taken together, these data indicate

that MHCII$^+$ ILC3s select for antigen specific RORγt$^+$ Tregs, and that this occurs in part by ILC3 expression of the $\alpha v\beta 3$ integrin, which can process latent TGF-β and interact with other extracellular ligands that could be important in this process.

Altered ILC3-Treg interactions in IBD

IBD is a human disease characterized by chronic inflammation of the GI tract with a substantial alteration in numbers or functionality of ILC3s[4,35,41–43] and RORγt$^+$ T lymphocytes[44–49]. However, a comprehensive definition of ILC3s and RORγt$^+$ T cell interactions in human health and IBD is lacking. This provoked us to perform scRNA-seq on the ILC and T cell compartments from the inflamed intestine versus adjacent non-inflamed intestine in human IBD (Extended Data Fig. 9a). Seventeen clusters were identified and visualized by UMAP (Fig. 5a). We separated the clusters of immune cells into T cells versus non-T cells as determined by expression of *CD3E* (Extended Data Fig. 10a). Among non-T cells, cluster 4 was identified as ILC3s by expression of *ID2, KIT* and *RORC* (Fig. 5b), and representation of these cell types was reduced in the inflamed tissue relative to adjacent non-inflamed tissue (Extended Data Fig. 10b). This decrease of ILC3s in the inflamed human intestine was associated with a significant decrease in expression of genes associated with ILC3 identity including *RORC, RORA, KIT, IL1R1, CCR6, IL22*, and those involved in antigen processing and presentation including *CD74, HLA-DRA, CD83, CD81, CTSH, IRF4* (Fig. 5c). Further, this impairment of ILC3s during intestinal inflammation was independently validated with colonic biopsies from a cohort of pediatric Crohn's disease patients relative to age-matched controls (Fig. 5d, Extended Data Fig. 9b). Among the T cells, cluster 6 and 8 were identified as Tregs by expression of *CD4* and *FOXP3* (Fig. 5e). A direct comparison of differentially expressed genes revealed that cluster 6 represents RORγt$^+$ Tregs as they displayed higher expression of *RORA, RORC, CCR6* and *CXCR6*, while cluster 8 exhibit features of thymic-derived Tregs with higher expression of HELIOS/ *IKZF2* (Fig. 5f, Supplementary Table 2). Representation of RORγt$^+$ Tregs (cluster 6) was also reduced in the inflamed human intestine relative to matched non-inflamed tissue, and this was associated with a significant decrease in genes associated with RORγt$^+$ Treg identity, function and TCR signaling (Fig. 5g, h). Several of these changes in abundance or transcriptional signatures among ILC3s and Tregs were found in another published data set from human IBD samples[44] (Extended Data Fig. 10c–e). Further, a significant reduction in the frequency of RORγt$^+$ Tregs was independently validated in colonic biopsies from a cohort of pediatric Crohn's disease patients relative to age-matched controls (Fig. 5i, Extended Data Fig. 9b, Supplementary Table 3). Finally, there was a modest but significant positive correlation between the frequency of ILC3s and the frequency of RORγt$^+$ Tregs in all analyzed intestinal biopsies (Fig. 5j, Extended Data Fig. 10f). Comparable results were validated in a second independent cohort of pediatric Crohn's disease patients (Extended Data Fig. 10g–i). These correlative data suggest that ILC3s promote RORγt$^+$ Tregs to support intestinal health in humans, and these cellular interactions become altered in IBD.

Our collective data sets indicate that LTi-like ILC3s critically select for RORγt$^+$ Tregs and against Th17 cells to orchestrate immunologic tolerance to microbiota and maintain intestinal homeostasis (Extended Data Fig. 10j), which substantially broadens our current understanding of intestinal selection[26,32] and mucosal immunology. This likely occurs

after initial priming by DCs or other redundant antigen presenting cells in response to colonization with microbes, impacts T cells with distinct antigen-specificities, and requires antigen presentation via MHCII on LTi-like ILC3s with contributions from Itgav and gradients of competition for IL-2. The αvβ3 integrin could support processing of latent TGF-β or interact with other extracellular ligands. These are important findings in the emerging paradigm that there is sophisticated cross-regulation between RORγt$^+$ lymphocytes during homeostasis, which is essential to preserve the ability to rapidly respond to intestinal injury, infection, or inflammation. We further phenotypically define distinctions between ILC3s and RORγt$^+$ eTACs. A prior study defined that *in vitro* RANK-RANKL stimulation supports interconverting potential of these two cell types[19], raising the possibility that RORγt$^+$ eTACs contribute to these pathways at distinct developmental windows and during infection or inflammation. However, our results demonstrate that LTi-like ILC3s are non-redundant in selecting for microbiota specific RORγt$^+$ Tregs. We also identify a positive correlation between ILC3s and RORγt$^+$ Tregs in the human intestine, and a fundamental disruption of these cell types in IBD. Intriguingly, each of these RORγt$^+$ populations express IL-17, IL-23R and integrin α4β7, and it will be important to consider how targeting these molecules with currently available biologic therapies impacts these cellular pathways. Taken together, these findings fundamentally advance our understanding of the heterogeneity and functional interactions by which RORγt$^+$ cells coordinate intestinal health and immune tolerance to the microbiota. Our data indicate that disruption of ILC3s in human IBD inherently underlies the dysregulation of microbiota specific RORγt$^+$ Tregs and Th17 cells, thus shifting the balance from tolerance to inflammation. Defining strategies to prevent this impairment of ILC3s, or promote their expansion, may hold the key to reinstating tolerance to microbiota in human IBD. Finally, as we have shown[50], it is possible that MHCII$^+$ ILC3s could be harnessed to achieve antigen specific tolerance through a similar induction of Tregs in many autoimmune and related chronic inflammatory diseases.

Materials and methods

Data reporting

Animal sample size estimates were determined using power analysis (power = 90% and α = 0.05) based on the mean and standard deviation from our previous studies and/or pilot studies using at least three animals per group. No randomization method was used in animal experiments, because littermate group allocation was performed via animal genotypes; because of this, the investigators were not blinded to allocation during experiments.

Mice.—C57BL/6J mice, Thy1.1 transgenic mice, CD45.1 transgenic mice, Rosa-26-loxP-flanked STOP yellow fluorescent protein gene (eYFP) mice[51], *H2-Ab1*$^{fl/fl}$ mice[52], Red5-cre (*Il5*^{Cre}) mice[53], *Foxp3*^{Cre} mice[54], *Cd4*^{Cre} mice[55], *Itgax*^{Cre} (*Cd11c*^{Cre}) mice[56], *Clec9a*^{Cre} mice[57], *Il22*^{Cre} mice[58], *Rorc*$^{fl/fl}$ mice[59], *Itgav*$^{fl/fl}$ mice[60], SFB (7B8) TCR transgenic mice[33] and *H. hepaticus* (HH7-2) TCR transgenic mice[34] were purchased from the Jackson Laboratories. *Rorc*^{Cre} mice and *Rorc(γt)-Gfp*^{TG} (RORγt-eGFP) mice[61] were provided by Gerard Eberl. *Aire*^{Cre} mice[62] were provided by Yong Fan. MHCII$^{\Delta ILC3}$ mice were generated as previously described[32]. MHCII^{ILC3+} mice were generated by crossing *Rorc*^{Cre} mice with IAb^{b}STOP$^{fl/fl}$ mice[63] kindly provided by Terri M. Laufer. *Ncr1*^{Cre} mice[64] were

kindly provided by Eric Vivier (Inserm). *Il7r*^{Cre} mice[65] were kindly provided by David Artis (Weill Cornell Medicine) with permission from H.R. Rodewald. *Il2*$^{fl/fl}$ mice[66] were kindly provided by Kendall Smith (Weill Cornell Medicine). All mice were on a C57BL/6 background and maintained in specific pathogen-free facilities in Weill Cornell Medicine. Male and female mice were used at 5 to 12 weeks of age. All protocols were approved by the Institutional Animal Care and Use Committee at Weill Cornell Medicine, and all experiments were performed in accordance with its guidelines.

Flow cytometry and cell sorting.—Single cell suspensions were incubated on ice with conjugated antibodies in PBS containing 2% FBS and 1 mM EDTA. Unlabeled anti-CD16/32 (clone 2.4G2, BD biosciences) was used to block Fc receptors when analyzing myeloid cells. Dead cells were excluded with Fixable Aqua Dead Cell Stain (Thermo Fisher Scientific). The staining antibodies for flow cytometry were mainly purchased from Thermo Fisher Scientific, Biolegend or BD Biosciences. For mouse cell-surface staining: CCR6 (29-2L17), NKp46 (29A1.4), CD3ε (145-2C11), CD4 (RM4-5, GK1.5), CD5 (53-7.3), CD8α (53-6.7), CD11b (M1/70), CD11c (N418), CD19 (1D3), Gr1 (RB6-8C5), Ly-6G (1A8), CD45R/B220 (RA3-6B2), CD45.1 (A20), CD45.2 (104), CD45 (30-F11), CD64 (X54-5/7.1), CD90.1 (OX-7), CD90.2 (30-H12), CD127 (A7R34), CD51 (RMV-7), F4/80 (BM8), FcεR1α (MAR-1), MHC-II (M5/114.15.2), NK1.1 (PK136), TCRγδ (GL3), KLRG1 (2F1/KLRG1), CD44 (IM7), CD62L (MEL-14), CD25 (PC61), CXCR6 (SA051D1), Siglec-G (SH1), CD26 (H194-112), Nur77 (12.14), CD172α (P84), XCR1 (ZET), Ly-6C (HK1.4), CD132 (TUGm2), CD138 (281-2), CD117 (ACK2), CD122 (TM-β1), Sca-1 (D7), and Integrin α4β7 (DATK32). For mouse intracellular staining: FoxP3 (FJK-16S), GATA3 (L50-823), IL-17A (17B7), IFNγ (XMG1.2), Ki-67 (SolA15), Bim (C34C5), RORγt (B2D) and T-bet (4B10). Lineage markers for mouse are: CD3ε, CD5, CD19, B220, Gr1, NK1.1, CD11b, CD11c. For human samples cell-surface staining: CD3 (UCHT1), CD11c (3.9), CD14 (TuK4), CD19 (HIB19), CD34 (581), CD4 (SK3), CD45 (HI30), CD25 (BC96), CD94 (DX22), CD117 (104D2), CD123 (6H6), CD127 (A019D5), FcεR1 (AER-37(CRA1)) and NKp44 (44.189). For human samples intracellular staining: FOXP3 (PCH101), HELIOS (22F6). Human RORγt^{+} Tregs were gated as CD45^{+}CD3^{+}CD4^{+}FOXP3^{+}HELIOS^{-}RORγt^{+}, human ILC3s were gated as CD45^{+}CD3^{-}CD11c^{-}CD14^{-}CD19^{-}CD34^{-}CD94^{-}CD123^{-}FcεR1^{-}CD127^{+}CD117^{+}.

For intracellular staining, cells were fixed and permeabilized with FoxP3/Transcription Factor Staining Buffer Set following manufacture's instruction (Thermo Fisher Scientific). Briefly, cells were incubated with Foxp3 Fixation/Permeabilization working solution for 30 min at room temperature or overnight at 4°C, then stained with intracellular targets by incubating with following conjugated antibodies in 1X Permeabilization Buffer for 30 min at room temperature. For intracellular cytokine staining, cells were first incubated for 4 h in RPMI with 10% FBS, 50 ng/ml phorbol 12-myristate 13-acetate (PMA), 750 ng/ml ionomycin and 10 μg/ml brefeldin A, all obtained from Sigma Aldrich. Antibodies for flow cytometry were purchased from BioLegend, Thermo Fisher Scientific or BD Biosciences. IL-2 binding capacity was assessed using a biotinylated IL-2 fluorokine assay kit (R&D Systems), following the manufacturer's instructions. Flow cytometry data collection was

performed with an LSR Fortessa (BD Biosciences) and analyzed with FlowJo V10 software (Tree Star, Inc). Cell sorting was performed with an Aria II (BD Biosciences).

Quantitative PCR.—Sort-purified cells were lysed in RLT buffer (Qiagen). RNA was extracted via RNeasy mini kits (Qiagen), as per the manufacturer's instructions. Reverse transcription of RNA was performed using Superscript reverse transcription according to the protocol provided by the manufacturer (Thermo Fisher Scientific). Real-time PCR was performed on cDNA using SYBR green chemistry (Applied Biosystems). Reactions were run on a real-time PCR system (ABI 7500; Applied Biosystems). Samples were normalized to *Hprt1* and displayed as a fold change compared to controls.

Preparation of single cell suspensions from intestine or lymph nodes.—Small intestine, cecum and colon were removed, opened longitudinally, and rinsed with ice-cold PBS. Peyer's patches were removed from small intestine. Dissected intestinal tissues were cut into approximately 1.5 cm pieces and intestinal epithelial cells were dissociated by incubating in HBSS (Sigma-Aldrich) containing 5 mM EDTA (Thermo Fisher Scientific), 1 mM DTT (Sigma-Aldrich) and 2% FBS with shaking at 200 rpm for 20 min at 37°C. Epithelial cells dissociation was performed twice. Samples were vortexed and rinsed with PBS after each step. Epithelial cells fraction was discarded. Remaining tissues were enzymatically digested in RPMI containing 0.4 U/mL dispase (Thermo Fisher Scientific), 1 mg/mL collagenase III (Worthington), 20 μg/mL DNase I (Sigma-Aldrich) and 10% FBS on a shaker for 45 min at 37°C. Leukocytes were enriched by 40% (for flow cytometry) or 40%/80% (for sorting) Percoll (GE Healthcare) gradient centrifugation. Mesenteric lymph nodes were chopped and incubated in RPMI containing 2% FBS and 2 mg/mL Collagenase D (Sigma-Aldrich) with shaking at 200 rpm for 20 min at 37°C, cells were then dissociated using a pasteur pipette, and filtered through 70 μm cell strainer in PBS containing 0.5 mM EDTA and 2% FBS.

Adoptive transfer of microbiota specific TCR transgenic T cells.—Recipient mice ($CD45.2^+$, $CD90.2^+$) were colonized with *H. Hepaticus* (ATCC 51449/Hh3B1) by oral gavage 7 days before T cell transfer as described previously[34]. In some experiments antibiotics (1 g/L ampicillin, 1 g/L colistin, 5 g/L streptomycin in drinking-water for 3 days) were applied to permit robust colonization of *H. Hepaticus*. SFB is continuously colonizing mice in our facility. Naïve $CD4^+$ T cells of *H. hepaticus*-specific ($CD45.1^+$, $CD90.2^+$) and SFB-specific ($CD45.2^+$, $CD90.1^+$) mice were isolated from spleen and lymph nodes by a naïve $CD4^+$ T cell isolation kit following manufacturer's instructions (Miltenyi Biotech) or by a FACSAria cell sorter (BD Biosciences) gated as $CD45^+CD3^+CD4^+CD25^-CD44^{low}CD62L^{high}$. Recipient mice received 10,000-100,000 cells/mouse of both TCR transgenic $CD4^+$ T cells retro-orbitally and were analyzed 2 weeks after transfer.

Immunofluorescence and image analysis.—Tissue sections from experimental mice were cut and stained as described previously[67,68]. Briefly, 6-μm-thick sections of tissue were cut, fixed in cold acetone at 4°C for 20 min and then stored at −20°C before staining. The detection of RORγt in frozen tissue sections using immunofluorescence has been described

previously[69]. Antibodies raised against the following mouse antigens were used: purified Armenian hamster anti-mouse CD3 (clone 145-2C11, 1:100, Biolegend), CD11c (Clone HL3 - Isotype, 1:100, BD Pharmingen™), rat anti-mouse IL-7Rα eFluor660 (clone A7R34, 1:25, Thermo Fisher), biotin anti-mouse FOXP3 (clone: FJK-16s, 1:50, Thermo Fisher) and rat anti-mouse RORγt (clone AFKJS-9, 1:25, Thermo Fisher). Detection of RORγt expression required amplification of the signal as described previously[69]. Purified RORγt antibodies were detected with donkey anti-rat-IgG-FITC (1:150, Jackson ImmunoResearch), and then rabbit anti-FITC-AF488 (1:200, Invitrogen) and then with donkey anti-rabbit-IgG-AF488 (1:200, Invitrogen). Purified anti-CD3 antibodies were detected with DyLight™ 594 goat anti-Armenian hamster IgG (clone Poly4055, 1:200, Biolegend) and biotinylated FOXP3 antibodies were detected with SA-AF555 (1:500, Invitrogen). Sections were counterstained with DAPI (Invitrogen) and mounted using ProLong Gold (Invitrogen). Slides were analyzed on a Zeiss 780 Zen microscope (Zeiss). High resolution (x63) pictures of the interfollicular areas were taken. The number of RORγt$^+$ Tregs was enumerated using the Zen software (Zeiss). This was performed by examining 8 to 12 images of interfollicular zones from at least 3 individual mice. For each RORγt$^+$ Treg in the image was then quantified as either ‘adjacent’ or ‘not adjacent’ to an ILC3 based on observed co-localization of markers on the surface membrane (CD3 for T cell membrane and IL-7R but not CD3 for ILC3 membrane in this context, in addition to intracellular transcription factors).

***Ex vivo* ILC3 and T cell culture.—**T cell stability assay was conducted as previously reported[70] with minor modifications. Sort-purified RORγt$^+$ CD4$^+$ T cells (CD45$^+$RORγtGFP$^+$CD5$^+$CD3$^+$CD4$^+$) and ILC3s (CD45$^+$RORγtGFP$^+$CD3$^-$CD5$^-$CD19$^-$B220$^-$TCRγδ$^-$Gr1$^-$NK1.1$^-$CD11b$^-$CD11c$^-$CD127$^+$CCR6$^+$) were plated in a round-bottom 96-well plate at a 1:1 or 2:1 ratio (10^4 to 10^5 cells per well). In some experiments, technical replicates were necessarily used instead of biological replicates when cell numbers were limited. No statistical analyses were made when using technical replicates. Large intestine and mLN were used to collect RORγt$^+$ CD4$^+$ T cells and ILC3s. Cells were incubated in RPMI, supplemented with 10% FBS, 1 mM Sodium Pyruvate, 10 mM HEPES, 2 mM GlutaMax, 80 μM 2-mercaptoethanol, 100 U/mL penicillin, 100 μg/mL streptomycin (all from Thermo Fisher Scientific), 10 ng/mL recombinant IL-7 (Thermo Fisher Scientific), anti-integrin αV (Biolegend), anti-integrin β1 (BD Biosciences), anti-integrin β3 (BD Biosciences) and anti-integrin αVβ6 (MilliporeSigma) at 10 μg/mL at 37°C and 5% CO_2 for 72 hours. Cells were analyzed by flow cytometry.

Single cell RNA-Sequencing.—CD45$^+$TCRβ$^+$GFP$^+$ (T cells) and CD45$^+$TCRβ$^-$GFP$^+$ (non-T cells) were sorted from the mLN of RORγt-eGFP mice and mixed equally at 1:1 ratio to enrich the non-T cell populations. CD45$^+$CD19$^-$CD14$^-$CD123$^-$FcεRIα$^-$CD34$^-$CD94$^-$CD4$^-$CD127$^+$ILCs and CD45$^+$CD3$^+$ T cells were sorted from the resection of inflamed Crohn’s disease patient versus adjacent tissue and mixed at 1:4 ratio. For human IBD samples, 13,072 cells from noninflamed tissue and 14,104 cells from inflamed tissue were sequenced and reported in the data sets. scRNA-Seq libraries were generated using the 10X Genomics Chromium system with 3’ version 3 chemistry. Libraries were sequenced on an Illumina NovaSeq instrument. Reads

were processed by 10X's Cell Ranger version 3.1.0 using the mm10 reference genome, resulting in a filtered HDF5 file. scRNA-Seq data were further processed and analyzed using R version 3.6.3 (R Core Team 2020) and the Seurat package version 3.2.3[71]. Specifically, Cell Ranger output was imported using the Read10X_h5 function. Seurat objects were created using only genes appearing in at least 3 cells. Cells were further filtered to exclude those with fewer than 600 genes detected, more than 5000 genes detected, or more than 10 percent mitochondrial reads. Read counts were then normalized using the NormalizeData function. The graph representing cells with similar expression patterns was generated with the FindNeighbors function using the 20 largest principal components. Cell clusters were generated using the Louvain algorithm implemented by the FindClusters function with resolution parameter equal to 0.4. Marker genes for each cluster were determined using the Wilcoxon test on the raw counts, implemented by the function FindAllMarkers, and including only positive marker genes with log fold changes greater than 0.25 and Bonferroni-corrected p values less than 0.01. Cluster names were determined by manual inspection of the lists of cluster marker genes. Dimensionality reduction by Uniform Manifold Approximation and Projection was performed using the RunUMAP function with the 20 largest principal components. All visualizations of scRNA-Seq data were generated using the Seurat package as well as ggplot2 version 3.3.3[72].

Cell-cell interaction network.—Selected genes expressed in ILC3 clusters (2 and 12) as well as selected genes expressed in Treg clusters (0, 5, and 13) were submitted to the STRING database[73]. The resulting list of known protein-protein interactions was filtered to include only entries with either database annotations ("database_annotated") or experimental evidence ("experimentally_determined_interaction").

Human intestinal tissue isolation.—De-identified surgical resection intestinal tissues from an adult individual with Crohn's disease, or intestinal biopsies from the colon of pediatric individuals with Crohn's disease and sex- and age-matched controls with no IBD, were obtained following Institutional Review Board approved protocols from the JRI IBD Live Cell Bank Consortium at Weill Cornell Medicine (protocol number 1503015958). Informed consent was obtained from all subjects. Biopsies were cryopreserved in 90% FBS and 10% DMSO for future side-by-side comparison. Following thawing, tissues were incubated in 0.5 mg/ml collagenase D and 20 mg/ml DNase I for 1 hour at 37°C with shaking. After digestion, remaining tissues were further dissociated mechanically by a syringe plugger. Cells were filtered through a 70 mm cell strainer and used directly for staining.

Statistics.—P values of datasets were determined by unpaired two-tailed Student's t-test with 95% confidence interval for comparison between two independent groups. For repeated comparison between two groups, multiple unpaired two-tailed t-test was applied. For datasets that were not normally distributed, a Mann–Whitney U-test was performed. One-way ANOVA followed by Turkey's multiple comparison test was used for comparison between more than two groups. Simple linear regression was used to analyze correlation. All statistics were performed with GraphPad Prism version 9 (GraphPad Software Inc.). Investigators were not blinded to group allocation during experiments.

Extended Data

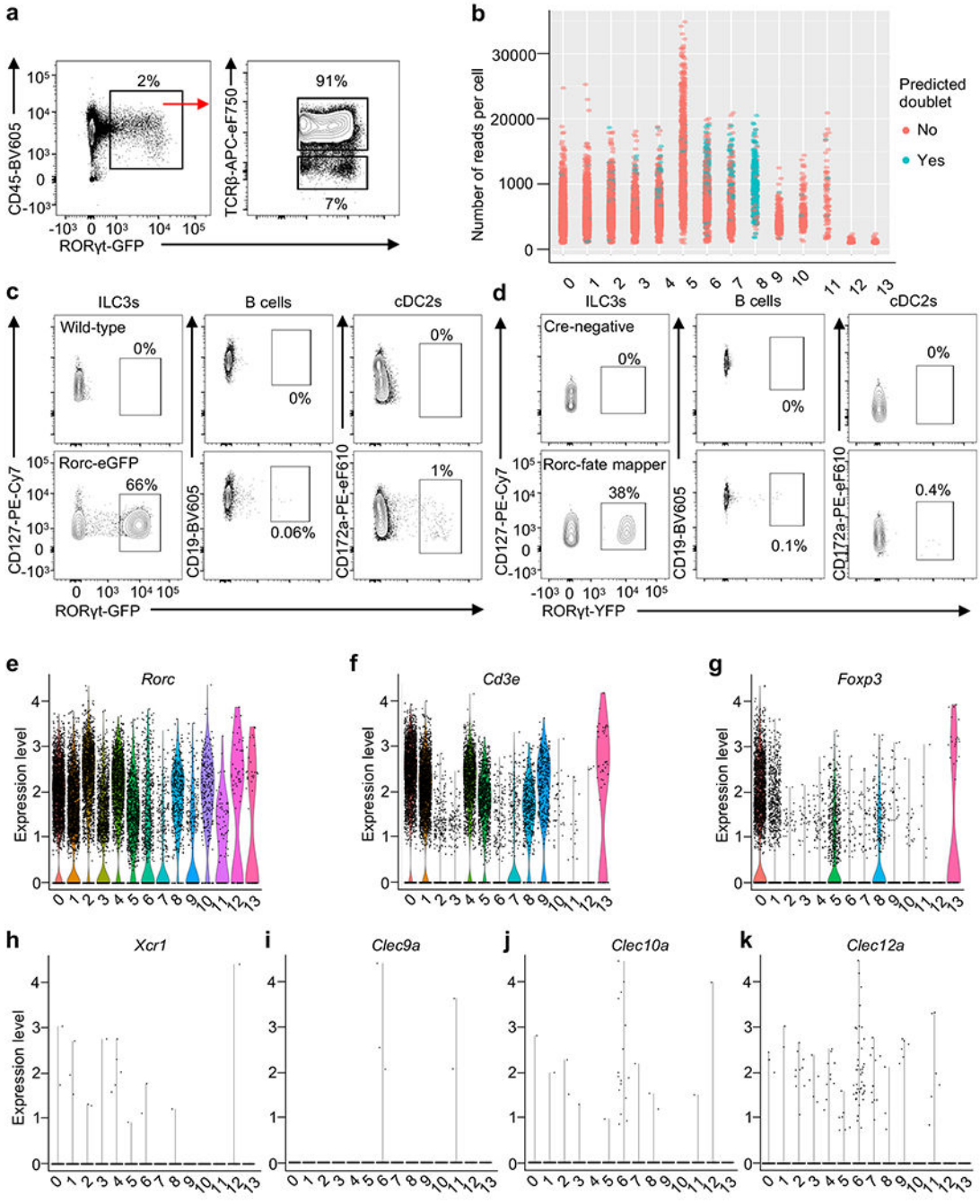

Extended Data Fig. 1 |. scRNA-seq profiling of RORγt$^+$ cells from mouse mLN.

a, Gating strategy to sort GFP$^+$TCRβ$^+$ and GFP$^+$TCRβ$^-$ cells (1:1, n = 3) for scRNA-seq. **b**, Doublet test showing cluster 8 as doublets. **c**, **d**, Representative flow cytometry plot of the frequency of RORγt$^+$ cells in CD127$^+$ ILC fractions (CD45$^+$CD3ε$^-$CD5$^-$NK1.1$^-$Ly6G$^-$TCRγ/δ$^-$B220$^-$CD11b$^-$CD11c$^-$KLRG1$^-$CD127$^+$), CD19$^+$ B cell fractions (CD45$^+$CD19$^+$) and CD172a$^+$ cDC2 fractions (CD45$^+$

CD3ε$^-$CD5$^-$NK1.1$^-$Ly6G$^-$TCRγ/δ$^-$B220$^-$CD64$^-$CD11c$^+$MHCII$^+$XCR1$^-$CD172a$^+$) from RORγt-eGFP reporter mice (n = 3) (**c**) and *Rorc*^{Cre} x Rosa26$^{lsl\text{-}YFP}$ fate mapped mice (n = 3) (**d**). **e-k**, Violin plot showing the expression of *Rorc* (**e**), *Cd3e* (**f**), *Foxp3* (**g**), *Xcr1* (**h**), *Clec9a* (**i**), *Clec10a* (**j**), *Clec12a* (**k**) among all the identified clusters.

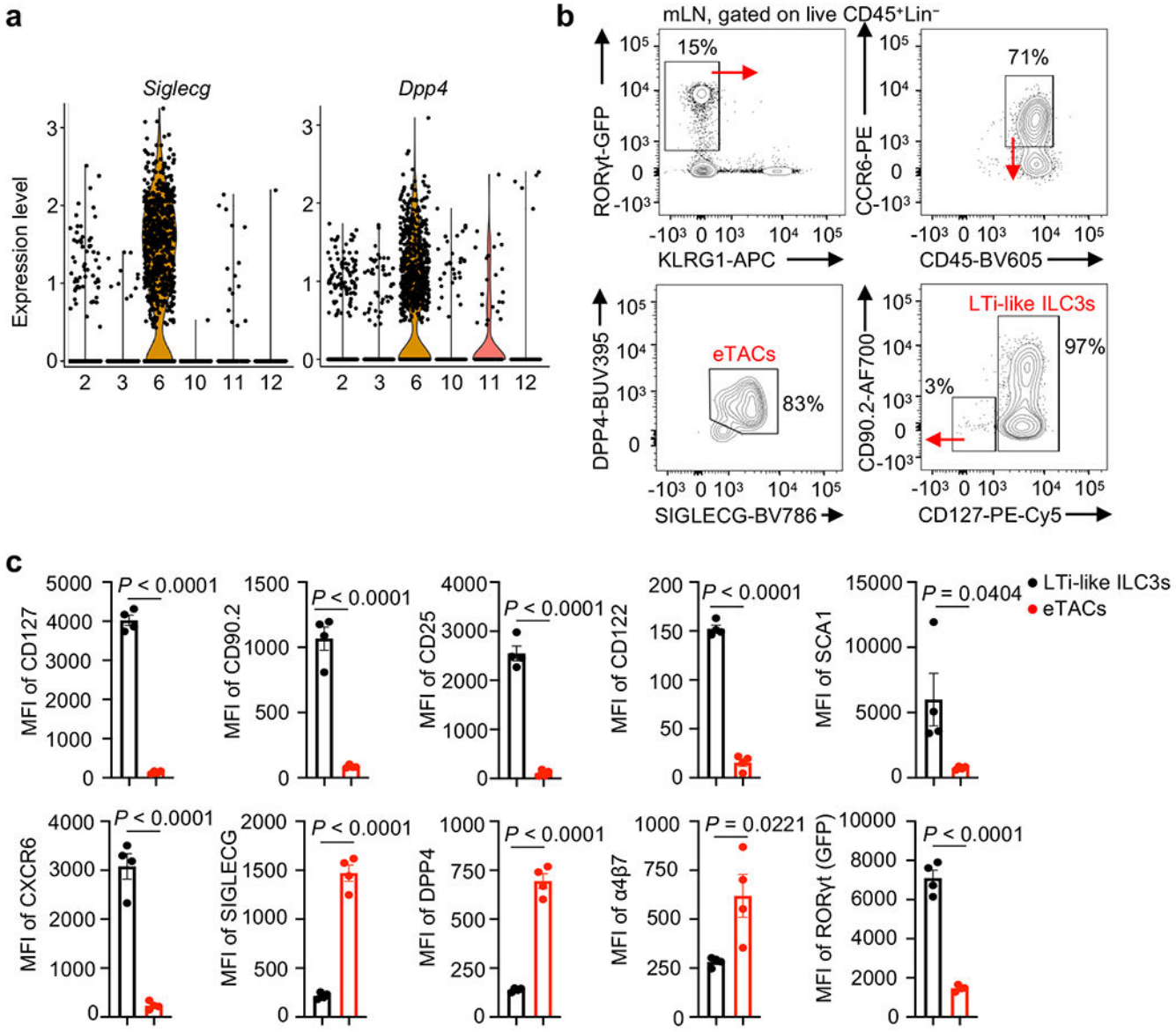

Extended Data Fig. 2 |. Characterization of RORγt$^+$ eTACs and LTi-like ILC3s in mouse mLN. **a**, Violin plot showing the expression of *Siglecg* and *Dpp4* among all the identified clusters of non-T lymphocytes. **b**, Gating strategy to identify ILC3s and RORγt$^+$ eTACs from mLN of RORγt-eGFP reporter mice (n = 4) for data shown in Fig. 1e, f. **c**, Quantification of indicated genes expression in LTi-like cells and RORγt$^+$ eTACs shown in Fig. 1e (n = 4). Data in **c** are representative of three independent experiments. Data are shown as means ± SEM, statistics shown in **c** are obtained by unpaired Student's *t*-test (two-tailed).

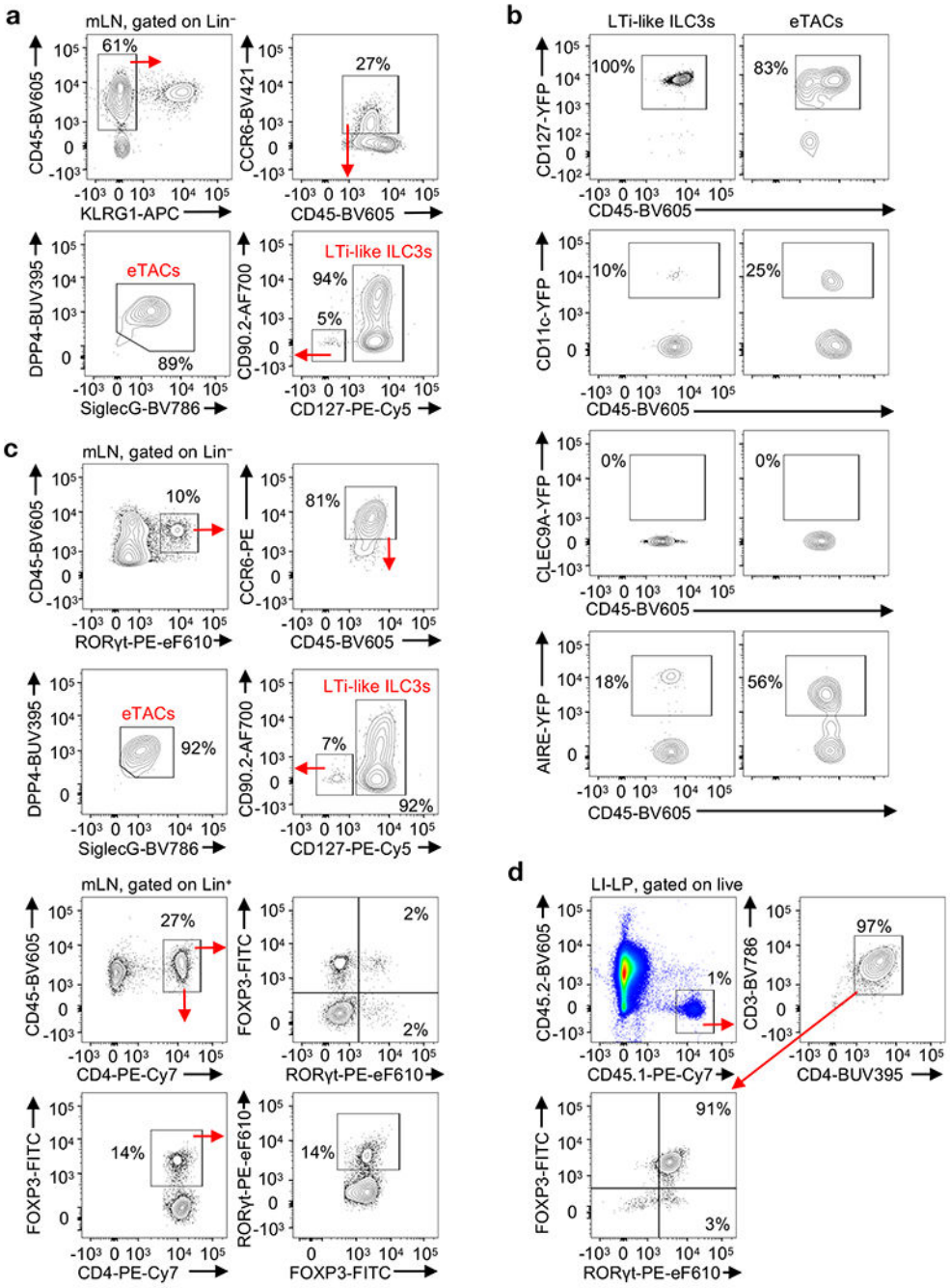

Extended Data Fig. 3 |. Gating strategies and fate mapping of RORγt$^+$ eTACs and LTi-like ILC3s in mouse mLN.

a, Gating strategy to identify LTi-like ILC3s and RORγt$^+$ eTACs for fate mapping analyses in Fig. 1g, h. **b**, Representative flow cytometry plots showing expression of CD127, CD11c, Clec9a and Aire among "fate-mapped" LTi-like ILC3s and RORγt$^+$ eTACs in mLN shown in Fig. 1g, h. **c**, Gating strategy to identify LTi-like ILC3s, RORγt$^+$ eTACs and RORγt$^+$ Tregs of mLN in Fig. 2c–l, Fig. 4e, the same gating strategy applied to the LI-LP. **d**, Gating strategy to identify *H. Hepaticus* (Hh)-specific CD4$^+$ T cells in mouse LI-LP.

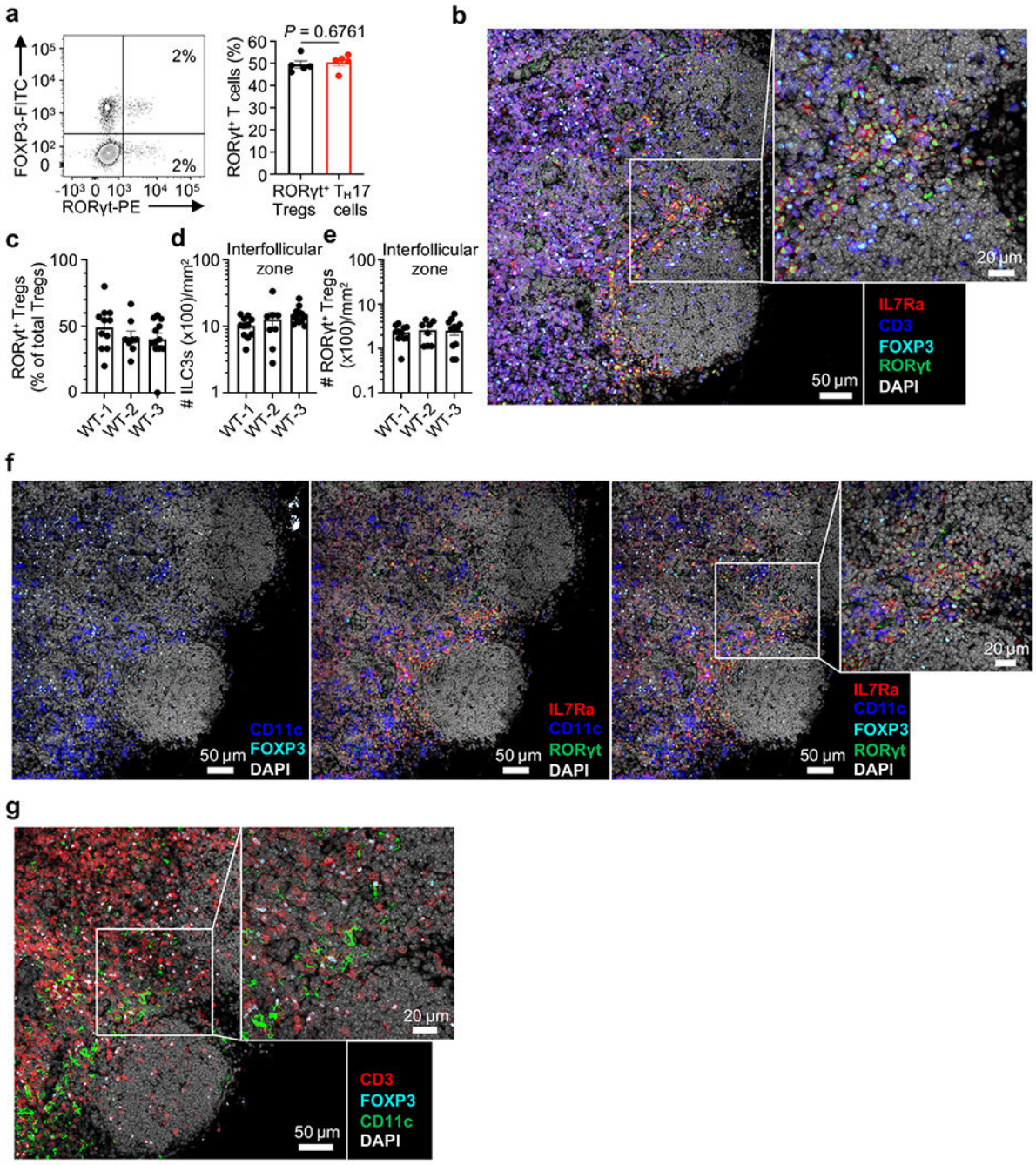

Extended Data Fig. 4 |. Immunofluorescence and quantification of different cell types in mLN. **a**, Representative flow cytometry plots of frequency (left) and percentage (right) of RORγt$^+$FoxP3$^+$ Tregs and RORγt$^+$FoxP3$^-$ Th17 cells among total RORγt$^+$CD4$^+$ T cells in mLN of WT mice (n = 5). **b**, Tile-scanned (left) and magnified (right) images of mLN stained for expression of IL7Rα (red), CD3 (blue), FOXP3 (cyan), RORγt (green) and DAPI (grey). **c-e**, Quantification of percentage of RORγt$^+$ Tregs among total Tregs (**c**), total numbers per mm^2 of ILC3s (**d**) and RORγt$^+$ Tregs (**e**) in interfollicular zone of mLN of WT-1 (n = 11 areas), WT-2 (n = 8 areas) and WT-3 (n = 12 areas) mice. **f**,

Tile-scanned images and serial sections of mLN stained for expression of IL7Rα (red), CD11c (blue), FOXP3 (cyan), RORγt (green) and DAPI (grey). Left panel is without IL7Rα and RORγt staining, middle panel is without FOXP3 staining, and right panel is a merge with a magnified image. **g**, Tile-scanned (left) and magnified (right) images of mLN stained for expression of CD3 (red), FOXP3 (cyan), CD11c (green) and DAPI (grey). Scale bars: 50 μm, 20 μm (in magnified images). Data in **a**, **b**, **f**, **g** are representative of two independent experiments. Data in **c**-**e** are representative of two independent experiments containing a total of 5 mice. Data are shown as means ± SEM, statistics shown in **a** are obtained by unpaired Student's *t*-test (two-tailed).

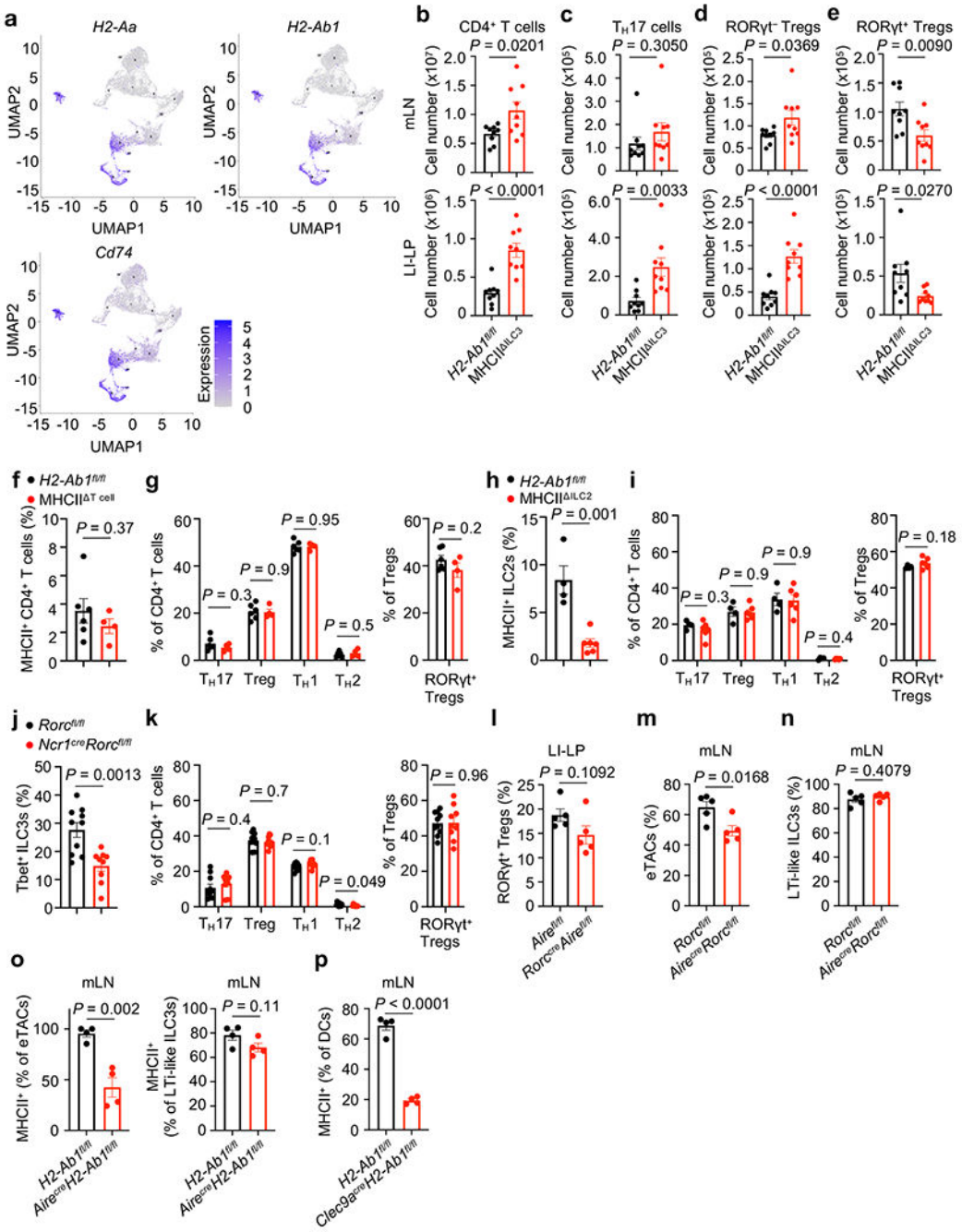

Extended Data Fig. 5 |. MHCII^{+} ILC3s selectively regulate T cell homeostasis in the gut.

a, UMAP plots of scRNA-seq data showing expression of *H2-Ab1*, *H2-Ab1* and *Cd74* are enriched in clusters of LTi-like ILC3s and RORγt^{+} eTACs across all the identified clusters in mouse mLN. **b-e,** Cell numbers of CD4^{+} T cells (**b**), Th17 cells (**c**), RORγt^{-}Tregs (**d**) and RORγt^{+} Tregs (**e**) in mLN (upper panel) and LI-LP (lower panel) of *H2-Ab1*$^{fl/fl}$ and MHCII$^{\Delta ILC3}$ mice (n = 8, pooled from 2 independent experiments). **f**-**k**, Large intestine of *H2-Ab1*$^{fl/fl}$ (n = 6) and *Cd4*^{Cre} *H2-Ab1*$^{fl/fl}$ (MHCII$^{\Delta T\ cell}$) mice (n = 4) (**f**, **g**), *H2-Ab1*$^{fl/fl}$ (n = 4) and *Il5*^{Cre} *H2-Ab1*$^{fl/fl}$ (MHCII$^{\Delta ILC2}$) mice (n = 6) (**h**, **i**), *Rorc*$^{fl/fl}$ (n = 10) and

Ncr1^{Cre} *Rorc*$^{fl/fl}$ mice (n = 9) (**j**, **k**) were analyzed. Proportion of MHCII-expressing CD4$^+$ T cells (**f**), ILC2s (**h**) and ILC3s (**j**). Frequency of each subset among CD4$^+$ T cells and RORγt$^+$ Tregs among total Tregs (**g, i, k**). Th17: Foxp3$^-$RORγt$^+$; Treg: Foxp3$^+$; Th1: Foxp3$^-$RORγ^-T-bet$^+$; Th2: Foxp3$^-$RORγt$^-$Gata3$^+$. **l**, Quantification of RORγt$^+$ Tregs among total CD4$^+$ T cells in LI-LP of *Aire*$^{fl/fl}$ and *Rorc*^{Cre}*Aire*$^{fl/fl}$ mice (n = 5). **m**, **n**, Quantification of eTACs among total CD127$^-$CD90$^-$ cells (**m**) and LTi-like ILC3s among CD45$^+$CCR6$^+$ cells (**n**) in mLN of *Rorc*$^{fl/fl}$ and *Aire*^{Cre}*Rorc*$^{fl/fl}$ mice (n = 5). **o**, Quantification of MHCII expression among eTACs (**o,** left) and LTi-like ILC3s (**o,** right) in mLN of *H2-Ab1*$^{fl/fl}$ and *Aire*^{Cre}*H2-Ab1*$^{fl/fl}$ mice (n = 4). **p**, Quantification of MHCII expression among DCs in mLN of *H2-Ab1*$^{fl/fl}$ and *Clec9a*^{Cre}*H2-Ab1*$^{fl/fl}$ mice (n = 4). Data are representative of two independent experiments unless otherwise indicated. Data shown as mean ± SEM. Statistics in **f**, **h**, **j**, **l-p,** right of **g, i, k** are obtained by unpaired Student's *t*-test. Statistics shown in left of **g**, **i**, **k** are obtained by multiple unpaired *t*-test. Statistics are calculated by two-tailed test.

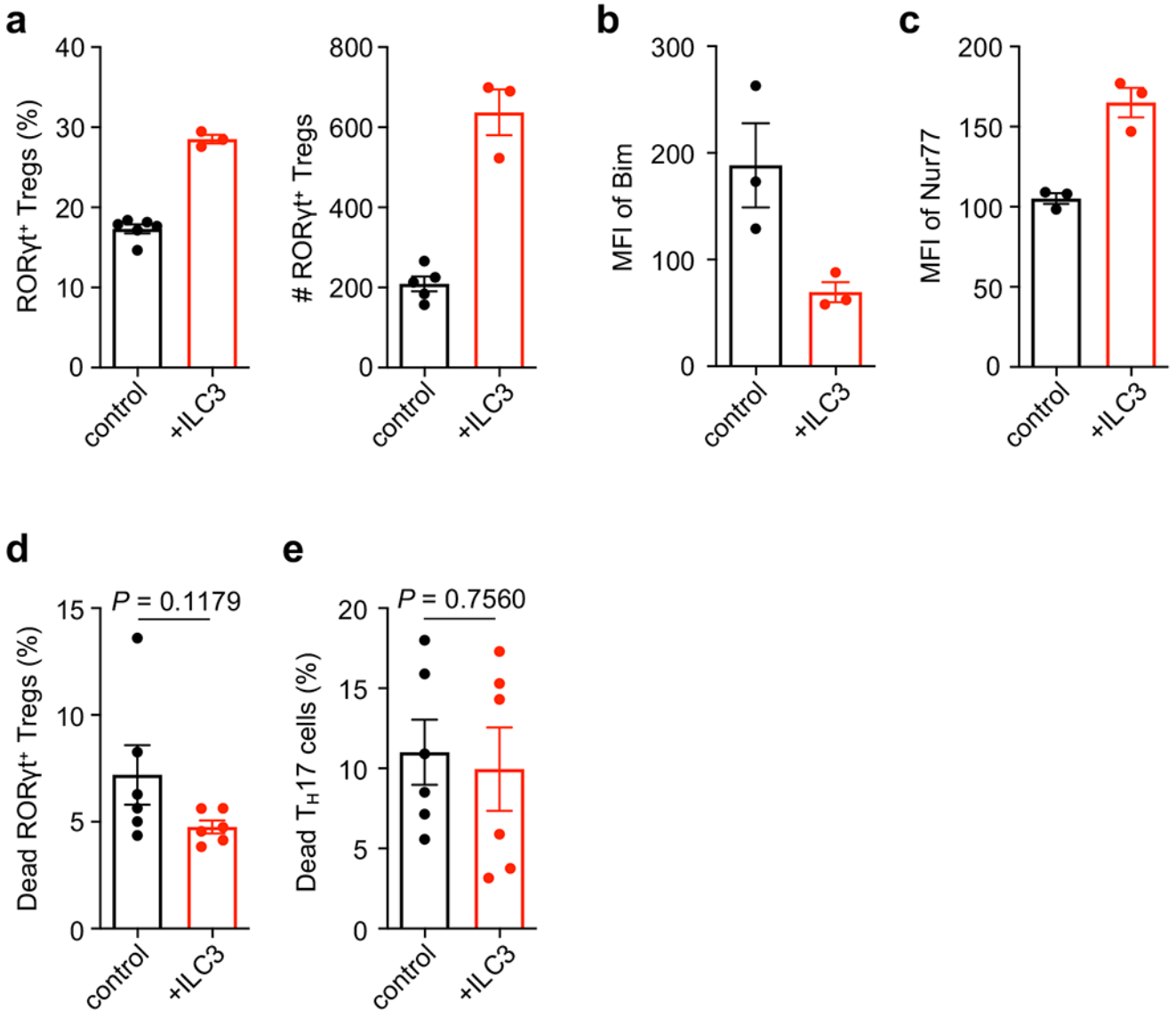

Extended Data Fig. 6 |. LTi-like ILC3s support RORγt$^+$ Tregs in a co-culture system.

a-c, Sort-purified RORγt$^+$CD4$^+$ T cells and LTi-like ILC3s from LI-LP and mLN (n = 6 or 5 or 3 per group as technical replicates) were co-cultured for 72 hours and RORγt$^+$ Tregs were analyzed by flow cytometry. Frequency and cell number of RORγt$^+$ Tregs (**a**, RORγt$^+$Foxp3$^+$ among CD4$^+$ T cells), MFI of Bim (**b**) and Nur77 (**c**) in RORγt$^+$ Tregs. **d**, **e**, Dead cells were quantified in RORγt$^+$ Tregs (**d**) and Th17 cells (**e**) after co-culture with or without LTi-like ILC3s for 72 hours. RORγt$^+$CD4$^+$ T cells and LTi-like ILC3s were sort-purified from mLN and LI-LP and pooled for co-culture assay (n = 12, each dot represents samples pooled from 2 mice). Data in **a-c** are representative of two independent experiments. Data in **d**, **e** are pooled from two independent experiments. Data are shown as mean ± SEM, statistics shown in **d**, **e** were obtained by unpaired Student's *t*-test (two-tailed).

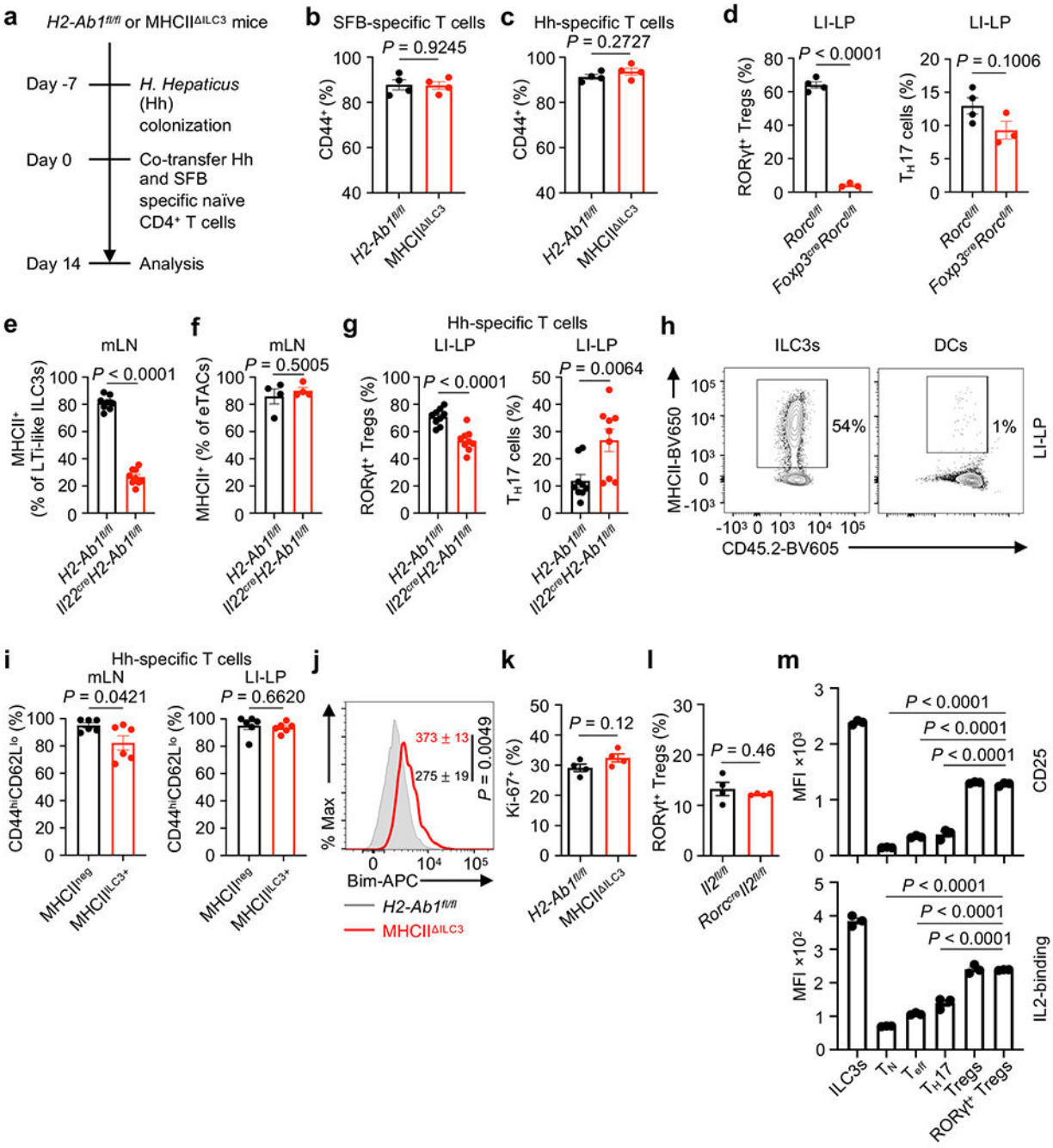

Extended Data Fig. 7 |. MHCII^{+} LTi-like ILC3s select for microbiota specific RORγt^{+} Tregs.
a, *H. hepaticus* (Hh)-specific and/or SFB-specific CD4^{+} T cells were transferred to *H2-Ab1*$^{fl/fl}$ and MHCII$^{\Delta ILC3}$ mice colonized with *H. hepaticus* 2 weeks before experiment as shown in Fig. 3 a–h, k, l. **b**, **c**, Frequency of CD44^{+} ratio among SFB-specific (**b**) or Hh-specific (**c**) CD4^{+} T cells were analyzed in Peyer's patch for SFB (CD45.1^{-}CD90.1^{+}CD4^{+} T cells) and in LI-LP for Hh-specific (CD45.1^{+}CD90.1^{-}CD4^{+} T cells) transgenic T cells (n = 4). **d**, Quantification of RORγt^{+} Tregs and Th17 cells among total CD4^{+} T cells in LI-LP of *Rorc*$^{fl/fl}$ and *Foxp3*^{Cre}*Rorc*$^{fl/fl}$ mice (n = 4). **e**, **f**, Quantification of MHCII expression

on LTi-like ILC3s (n = 9) (**e**) and eTACs (n = 4) (**f**) in mLN of *H2-Ab1*$^{fl/fl}$ and *Il22*^{Cre}*H2-Ab1*$^{fl/fl}$ mice. **g**, Quantification of RORγt^{+} Tregs (among Hh-specific CD4^{+} T cells) and Th17 cells (among Hh-specific CD4^{+} T cells) were analyzed in LI-LP of *H2-Ab1*$^{fl/fl}$ and *Il22*^{Cre}*H2-Ab1*$^{fl/fl}$ mice (n = 9). **h**, Representative flow cytometry plots of the frequency of MHCII expression on ILC3s, DCs in LI-LP of MHCII^{neg} and MHCII^{ILC3+} mice (n = 6) as shown in Fig. 3j. **i**, Frequency of CD44^{hi}CD62L^{lo} ratio among Hh-specific CD4^{+} T cells were analyzed in mLN and LI-LP for Hh-specific CD4^{+} T cells as shown in Fig. 3k, l (n = 6). **j**, **k**, RORγt^{+} Tregs in LI-LP of *H2-Ab1*$^{fl/fl}$ and MHCII$^{\Delta ILC3}$ mice (n = 4) were analyzed by flow cytometry. Histogram and MFI of Bim (**j**). Proportions of Ki-67 positive cells (**k**). **l**, Quantification of RORγt^{+} Tregs among CD4^{+} T cells in LI-LP of *Il2*$^{fl/fl}$ and *Rorc*^{Cre}*Il2*$^{fl/fl}$ mice (n = 4). **m**, Quantification of CD25 staining or IL-2 binding in mLN of WT mice (n = 3). Naive T cells: CD44^{lo}CD62L^{hi}; effector T: CD44^{hi}CD62L^{lo}; Th17 cells: RORγt^{+}FoxP3^{-}; Tregs: FoxP3^{+}; RORγt^{+}Tregs: RORγt^{+}FoxP3^{+}. Data in **e**, **g** are pooled from two independent experiments with similar results. Data in **b**-**d**, **f**, **i**-**l** are representative of two independent experiments. Data are shown as mean ± SEM, statistics shown in **m** are obtained by one-way ANOVA with Tukey's multiple comparisons test, statistics shown in **b**-**g**, **i**-**l** are obtained by unpaired Student's *t*-test (two-tailed).

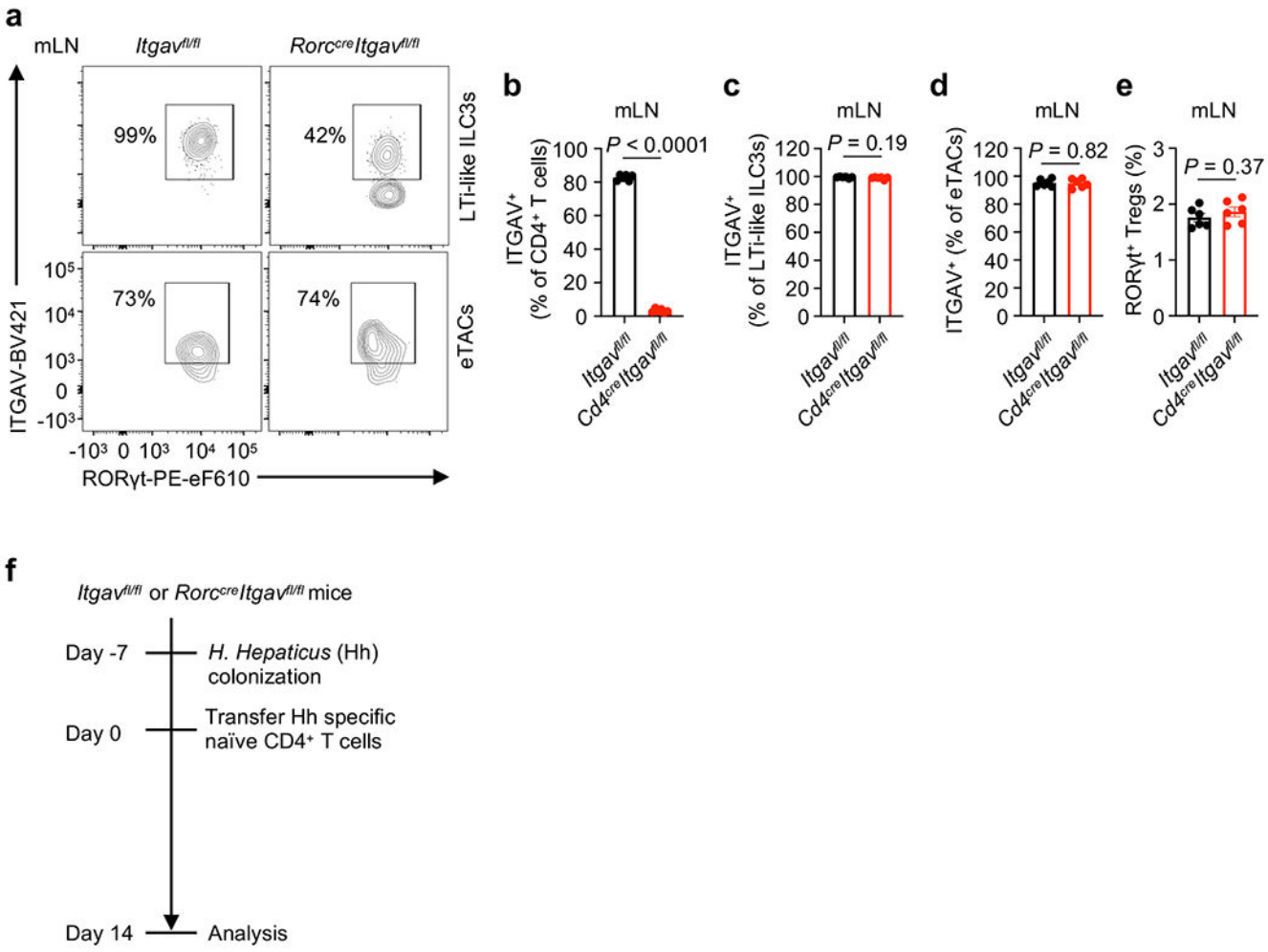

Extended Data Fig. 8 |. Itgav on LTi-like ILC3s contributes to the selection of microbiota-specific RORγt$^+$ Tregs.

a, Representative flow cytometry plot of the frequency of Itgav expression on LTi-like ILC3s and eTACs in mLN of *Itgav*$^{fl/fl}$ and *Rorc*^{Cre}*Itgav*$^{fl/fl}$ mice as shown in Fig. 4d (n = 5). **b**-**d**, Quantification of Itgav on CD4$^+$ T cells (**b**), LTi-like ILC3s (**c**) and eTACs (**d**) in mLN of *Itgav*$^{fl/fl}$ and *Cd4*^{Cre}*Itgav*$^{fl/fl}$ mice (n = 6). **e**, Quantification of RORγt$^+$ Tregs in mLN of *Itgav*$^{fl/fl}$ and *Cd4*^{Cre}*Itgav*$^{fl/fl}$ mice (n = 6). **f**, *H. Hepaticus* (Hh)-specific CD4$^+$ T cells were transferred to *Itgav*$^{fl/fl}$ and *Rorc*^{Cre}*Itgav*$^{fl/fl}$ mice colonized with *H. hepaticus* 14 days before experiment related to Fig. 4f. Data in **b**-**e** are representative of two independent experiments. Data are shown as mean ± SEM, statistics shown in **b**-**e** are obtained by unpaired Student's *t*-test (two-tailed).

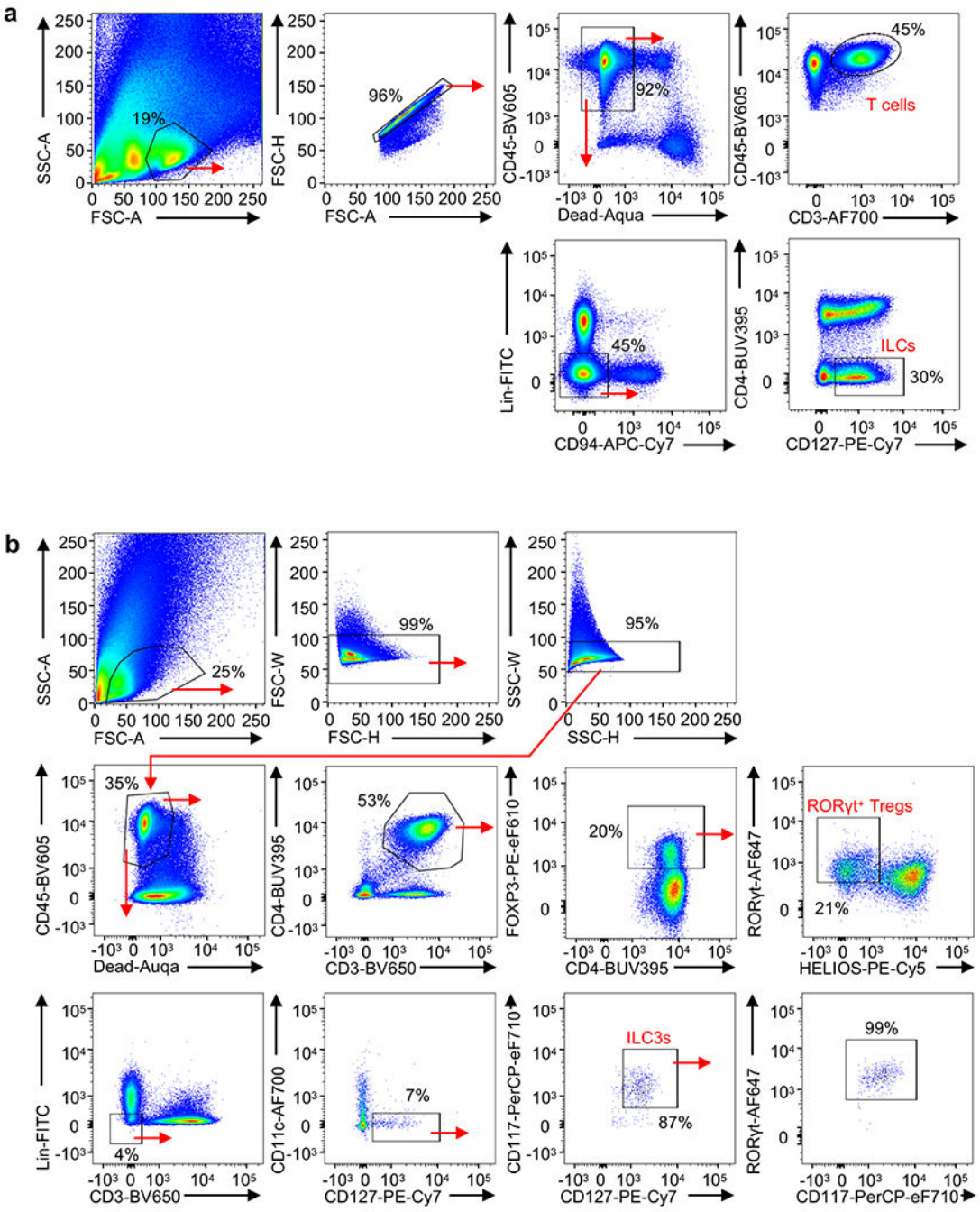

Extended Data Fig. 9 |. Gating strategy for ILC3s and T cell subsets in the human intestine.
a, Gating strategy to sort ILCs and T cells from small intestine of the IBD patient for scRNA-seq in Fig. 5. **b**, Gating strategy to demonstrate the ILC3s and RORγt^{+} Tregs shown in Fig. 5.

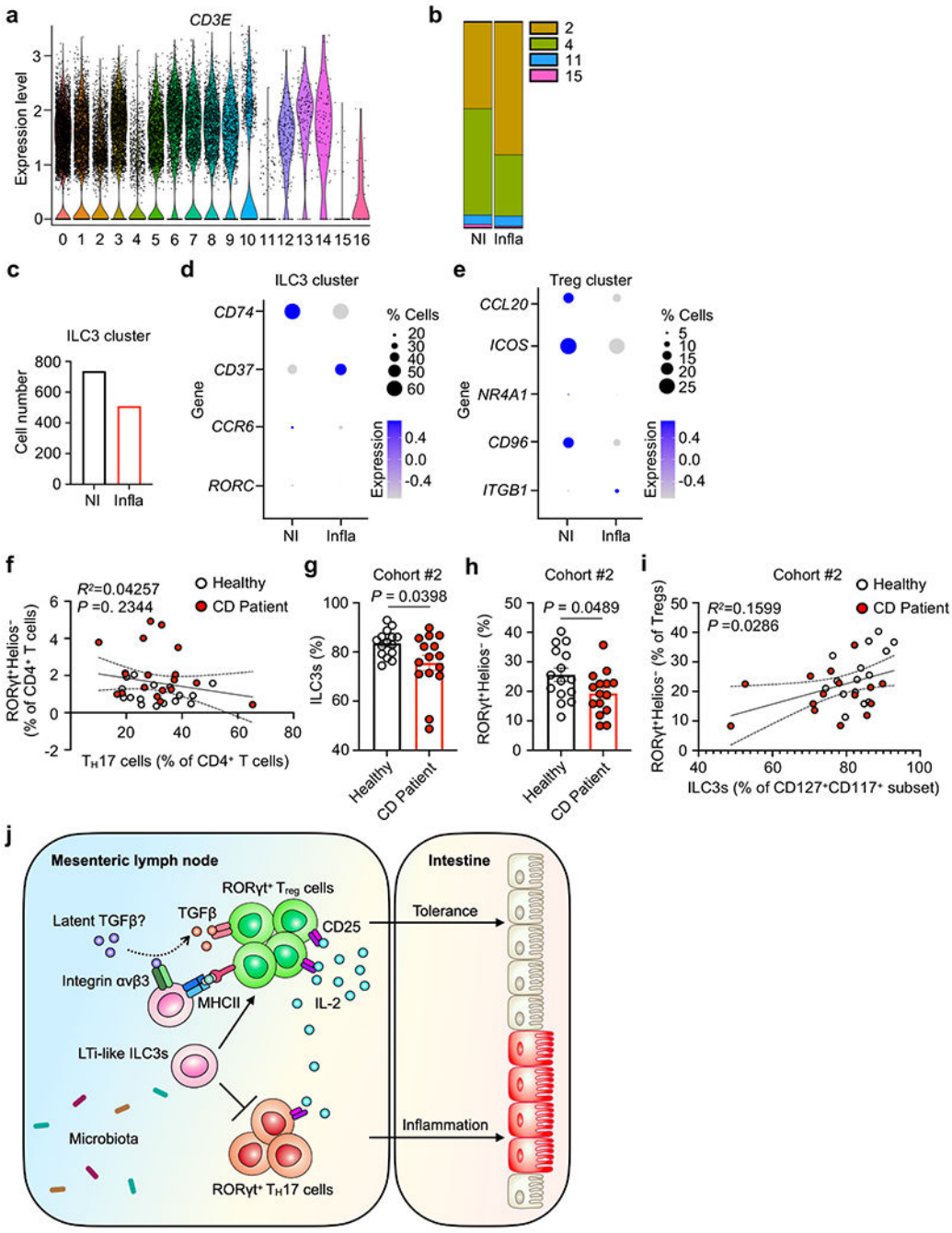

Extended Data Fig. 10 |. ILC3s select microbiota specific Tregs to establish tolerance in the gut.
a, Violin plot of *CD3E* expression among clusters of scRNA-seq data as shown in Fig. 5a. **b**, Bar graph showing the composition of non-T lymphocytes as indicated in Fig. 5a in non-inflamed tissue (NI) versus inflamed tissue (Infla). **c**, Bar graph showing the composition of ILC3 lymphocytes in non-inflamed tissue (NI) versus inflamed tissue (Infla) from human IBD samples as published[44]. **d**, **e**, A dot plot showing the mean expression (colour) of indicated genes in ILC3 cluster (**d**) and Treg cluster (**e**) in non-inflamed versus inflamed tissue from human IBD samples as published[44]. **f**, Correlation analyses between

the RORγt$^+$ Tregs (RORγt$^+$Helios$^-$ among CD4$^+$ T cells) and Th17 cells (RORγt$^+$FoxP3$^-$ among CD4$^+$ T cells) in the cohort of CD patients as in Fig.5d, i, j. **g, h,** Quantification of frequency of ILC3s among CD127$^+$CD117$^+$ subset (**g**) and RORγt$^+$ Tregs among total Tregs (**h**) in a second independent cohort of individuals. Healthy donor n = 15, Crohn's disease (CD) patients n = 15. **i**, Correlation analyses between the ILC3 (ILC3 among CD127$^+$CD117$^+$ subset) and RORγt$^+$ Tregs (RORγt$^+$ Helios$^-$ among FoxP3$^+$ Tregs) in a second independent cohort of human samples as in (**g**, **h**). **j**, LTi-like ILC3s are necessary and sufficient in selecting for the differentiation fate of microbiota specific RORγt$^+$ Tregs, and selecting against Th17 cells, via antigen presentation with contributions from integrin αv and gradients of competition for IL-2. This collectively enforces immunologic tolerance to microbiota and maintains intestinal homeostasis. Data in **g**, **h** are shown as means ± SEM, statistics shown in **g**, **h** are performed using Mann–Whitney *U*-test (unpaired), correlative analyses in **f, i** are compared by Pearson's rank correlation coefficient (R^2). Statistics are calculated by two-tailed test.

Supplementary Material

Refer to Web version on PubMed Central for supplementary material.

Acknowledgements

We thank members of the Sonnenberg Laboratory for discussions and critical reading of the manuscript. Research in the Sonnenberg Laboratory is supported by the National Institutes of Health (R01AI143842, R01AI123368, R01AI145989, U01AI095608, R21CA249274, R01AI162936 and R01CA274534), an Investigators in the Pathogenesis of Infectious Disease Award from the Burroughs Wellcome Fund, the Meyer Cancer Center Collaborative Research Initiative, the Dalton Family Foundation, and Linda and Glenn Greenberg. Wenqing Zhou, J.G., L.Z. and Wen Zhang are supported by fellowships from the Crohn's and Colitis Foundation (831404, 519428, 608975, and 901000, respectively). D.R.W. and F.G. are supported by a Senior Research Fellowship from the Wellcome Trust to DRW (110199/Z/15/Z). J.G.F. is supported by P30-ES002109 and R35CA210088. G.F.S. is a CRI Lloyd J. Old STAR. We would like to thank the Epigenomics Cores of Weill Cornell Medicine and G. Putzel for bioinformatics assistance, J. Conrad for administrative assistance, and S. Mozumder for technical assistance. The JRI IBD Live Cell Bank is supported by the JRI, Jill Roberts Center for IBD, Cure for IBD, the Rosanne H. Silbermann Foundation, the Sanders Family and Weill Cornell Medicine Division of Pediatric Gastroenterology, Hepatology, and Nutrition.

Data availability.

All data necessary to understand and evaluate the conclusions of this paper are provided in the manuscript and supplementary materials. scRNA-Seq data were deposited in the Gene Expression Omnibus database under the accession number GSE184175 and GSE184291. A re-analysis was performed on scRNA-Seq data publicly available with the accession number GSE134809. Source data are provided with this paper.

JRI Live Cell Bank consortium members

David Artis[3], Randy Longman[3], Gregory F. Sonnenberg[1,2,3], Ellen Scherl[3], Robbyn E. Sockolow[7], Dana Lukin[3], Robert Battat[3], Thomas Ciecierega[3], Aliza Solomon[3], Elaine Barfield[3], Kimberley Chien[3], Johanna Ferriera[3], Jasmin Williams[3], Shaira Khan[3], Peik Sean Chong[3], Samah Mozumder[3], Lance Chou[3], Wenqing Zhou[1,2,3], Anees Ahmed[3], Connie Zhong[3], Ann Joseph[3], Sanchita Kashyap[3], Joseph Gladstone[3] & Samantha Jensen[3]

References

1. Honda K & Littman DR The microbiota in adaptive immune homeostasis and disease. Nature 535, 75–84 (2016). [PubMed: 27383982]
2. Maloy KJ & Powrie F Intestinal homeostasis and its breakdown in inflammatory bowel disease. Nature 474, 298–306 (2011). [PubMed: 21677746]
3. Maynard CL, Elson CO, Hatton RD & Weaver CT Reciprocal interactions of the intestinal microbiota and immune system. Nature 489, 231–241 (2012). [PubMed: 22972296]
4. Zhou L & Sonnenberg GF Essential immunologic orchestrators of intestinal homeostasis. Sci Immunol 3 (2018).
5. Belkaid Y & Hand TW Role of the microbiota in immunity and inflammation. Cell 157, 121–141 (2014). [PubMed: 24679531]
6. Hooper LV & Macpherson AJ Immune adaptations that maintain homeostasis with the intestinal microbiota. Nat Rev Immunol 10, 159–169 (2010). [PubMed: 20182457]
7. Harrison OJ & Powrie FM Regulatory T cells and immune tolerance in the intestine. Cold Spring Harb Perspect Biol 5 (2013).
8. Janney A, Powrie F & Mann EH Host-microbiota maladaptation in colorectal cancer. Nature 585, 509–517 (2020). [PubMed: 32968260]
9. Harrington LE et al. Interleukin 17-producing CD4+ effector T cells develop via a lineage distinct from the T helper type 1 and 2 lineages. Nat Immunol 6, 1123–1132 (2005). [PubMed: 16200070]
10. Park H et al. A distinct lineage of CD4 T cells regulates tissue inflammation by producing interleukin 17. Nat Immunol 6, 1133–1141 (2005). [PubMed: 16200068]
11. Ohnmacht C et al. MUCOSAL IMMUNOLOGY. The microbiota regulates type 2 immunity through RORγt^+ T cells. Science 349, 989–993 (2015). [PubMed: 26160380]
12. Sefik E et al. MUCOSAL IMMUNOLOGY. Individual intestinal symbionts induce a distinct population of RORγ^+ regulatory T cells. Science 349, 993–997 (2015). [PubMed: 26272906]
13. Buonocore S et al. Innate lymphoid cells drive interleukin-23-dependent innate intestinal pathology. Nature 464, 1371–1375 (2010). [PubMed: 20393462]
14. Cella M et al. A human natural killer cell subset provides an innate source of IL-22 for mucosal immunity. Nature 457, 722–725 (2009). [PubMed: 18978771]
15. Sawa S et al. Lineage relationship analysis of RORgammat+ innate lymphoid cells. Science 330, 665–669 (2010). [PubMed: 20929731]
16. Spits H et al. Innate lymphoid cells--a proposal for uniform nomenclature. Nat Rev Immunol 13, 145–149 (2013). [PubMed: 23348417]
17. Eberl G RORgammat, a multitask nuclear receptor at mucosal surfaces. Mucosal Immunol 10, 27–34 (2017). [PubMed: 27706126]
18. Goc J et al. Dysregulation of ILC3s unleashes progression and immunotherapy resistance in colon cancer. Cell 184, 5015–5030.e5016 (2021). [PubMed: 34407392]
19. Yamano T et al. Aire-expressing ILC3-like cells in the lymph node display potent APC features. J Exp Med 216, 1027–1037 (2019). [PubMed: 30918005]
20. Cabeza-Cabrerizo M, Cardoso A, Minutti CM, Pereira da Costa M & Reis e Sousa C Dendritic Cells Revisited. Annu Rev Immunol 39, 131–166 (2021). [PubMed: 33481643]
21. Zhou W et al. ZBTB46 defines and regulates ILC3s that protect the intestine. Nature in press (2022).
22. Gardner JM et al. Extrathymic Aire-expressing cells are a distinct bone marrow-derived population that induce functional inactivation of CD4(+) T cells. Immunity 39, 560–572 (2013). [PubMed: 23993652]
23. Wells KL et al. Combined transient ablation and single-cell RNA-sequencing reveals the development of medullary thymic epithelial cells. Elife 9 (2020).
24. Anderson MS et al. Projection of an immunological self shadow within the thymus by the aire protein. Science 298, 1395–1401 (2002). [PubMed: 12376594]

25. Mackley EC et al. CCR7-dependent trafficking of RORgamma(+) ILCs creates a unique microenvironment within mucosal draining lymph nodes. Nat Commun 6, 5862 (2015). [PubMed: 25575242]
26. Hepworth MR et al. Immune tolerance. Group 3 innate lymphoid cells mediate intestinal selection of commensal bacteria-specific CD4^{+} T cells. Science 348, 1031–1035 (2015). [PubMed: 25908663]
27. Coombes JL et al. A functionally specialized population of mucosal CD103+ DCs induces Foxp3+ regulatory T cells via a TGF-beta and retinoic acid-dependent mechanism. J Exp Med 204, 1757–1764 (2007). [PubMed: 17620361]
28. Farache J et al. Luminal bacteria recruit CD103+ dendritic cells into the intestinal epithelium to sample bacterial antigens for presentation. Immunity 38, 581–595 (2013). [PubMed: 23395676]
29. Sun CM et al. Small intestine lamina propria dendritic cells promote de novo generation of Foxp3 T reg cells via retinoic acid. J Exp Med 204, 1775–1785 (2007). [PubMed: 17620362]
30. Tanoue T, Atarashi K & Honda K Development and maintenance of intestinal regulatory T cells. Nat Rev Immunol 16, 295–309 (2016). [PubMed: 27087661]
31. Russler-Germain EV et al. Gut Helicobacter presentation by multiple dendritic cell subsets enables context-specific regulatory T cell generation. Elife 10 (2021).
32. Hepworth MR et al. Innate lymphoid cells regulate CD4+ T-cell responses to intestinal commensal bacteria. Nature 498, 113–117 (2013). [PubMed: 23698371]
33. Yang Y et al. Focused specificity of intestinal TH17 cells towards commensal bacterial antigens. Nature 510, 152–156 (2014). [PubMed: 24739972]
34. Xu M et al. c-MAF-dependent regulatory T cells mediate immunological tolerance to a gut pathobiont. Nature 554, 373–377 (2018). [PubMed: 29414937]
35. Zhou L et al. Innate lymphoid cells support regulatory T cells in the intestine through interleukin-2. Nature 568, 405–409 (2019). [PubMed: 30944470]
36. Belkaid Y & Oldenhove G Tuning microenvironments: induction of regulatory T cells by dendritic cells. Immunity 29, 362–371 (2008). [PubMed: 18799144]
37. Worthington JJ, Czajkowska BI, Melton AC & Travis MA Intestinal dendritic cells specialize to activate transforming growth factor-beta and induce Foxp3+ regulatory T cells via integrin alphavbeta8. Gastroenterology 141, 1802–1812 (2011). [PubMed: 21723222]
38. Worthington JJ et al. Integrin alphavbeta8-Mediated TGF-beta Activation by Effector Regulatory T Cells Is Essential for Suppression of T-Cell-Mediated Inflammation. Immunity 42, 903–915 (2015). [PubMed: 25979421]
39. Ouyang W, Beckett O, Ma Q & Li MO Transforming growth factor-beta signaling curbs thymic negative selection promoting regulatory T cell development. Immunity 32, 642–653 (2010). [PubMed: 20471291]
40. Sarrazy V et al. Integrins αvβ5 and αvβ3 promote latent TGF-β1 activation by human cardiac fibroblast contraction. Cardiovasc Res 102, 407–417 (2014). [PubMed: 24639195]
41. Bernink JH et al. Human type 1 innate lymphoid cells accumulate in inflamed mucosal tissues. Nat Immunol 14, 221–229 (2013). [PubMed: 23334791]
42. Teng F et al. A circadian clock is essential for homeostasis of group 3 innate lymphoid cells in the gut. Sci Immunol 4 (2019).
43. Vivier E et al. Innate Lymphoid Cells: 10 Years On. Cell 174, 1054–1066 (2018). [PubMed: 30142344]
44. Martin JC et al. Single-Cell Analysis of Crohn's Disease Lesions Identifies a Pathogenic Cellular Module Associated with Resistance to Anti-TNF Therapy. Cell 178, 1493–1508 e1420 (2019). [PubMed: 31474370]
45. Hovhannisyan Z, Treatman J, Littman DR & Mayer L Characterization of interleukin-17-producing regulatory T cells in inflamed intestinal mucosa from patients with inflammatory bowel diseases. Gastroenterology 140, 957–965 (2011). [PubMed: 21147109]
46. Jaeger N et al. Single-cell analyses of Crohn's disease tissues reveal intestinal intraepithelial T cells heterogeneity and altered subset distributions. Nat Commun 12, 1921 (2021). [PubMed: 33771991]

47. Boland BS et al. Heterogeneity and clonal relationships of adaptive immune cells in ulcerative colitis revealed by single-cell analyses. Sci Immunol 5 (2020).
48. Smillie CS et al. Intra- and Inter-cellular Rewiring of the Human Colon during Ulcerative Colitis. Cell 178, 714–730 e722 (2019). [PubMed: 31348891]
49. Friedrich M, Pohin M & Powrie F Cytokine Networks in the Pathophysiology of Inflammatory Bowel Disease. Immunity 50, 992–1006 (2019). [PubMed: 30995511]
50. Grigg JB et al. Antigen-presenting innate lymphoid cells orchestrate neuroinflammation. Nature 600, 707–712 (2021). [PubMed: 34853467]
51. Srinivas S et al. Cre reporter strains produced by targeted insertion of EYFP and ECFP into the ROSA26 locus. BMC Dev Biol 1, 4 (2001). [PubMed: 11299042]
52. Hashimoto K, Joshi SK & Koni PA A conditional null allele of the major histocompatibility IA-beta chain gene. Genesis 32, 152–153 (2002). [PubMed: 11857806]
53. Nussbaum JC et al. Type 2 innate lymphoid cells control eosinophil homeostasis. Nature 502, 245–248 (2013). [PubMed: 24037376]
54. Rubtsov YP et al. Regulatory T cell-derived interleukin-10 limits inflammation at environmental interfaces. Immunity 28, 546–558 (2008). [PubMed: 18387831]
55. Lee PP et al. A critical role for Dnmt1 and DNA methylation in T cell development, function, and survival. Immunity 15, 763–774 (2001). [PubMed: 11728338]
56. Caton ML, Smith-Raska MR & Reizis B Notch-RBP-J signaling controls the homeostasis of CD8- dendritic cells in the spleen. J Exp Med 204, 1653–1664 (2007). [PubMed: 17591855]
57. Schraml BU et al. Genetic tracing via DNGR-1 expression history defines dendritic cells as a hematopoietic lineage. Cell 154, 843–858 (2013). [PubMed: 23953115]
58. Ahlfors H et al. IL-22 fate reporter reveals origin and control of IL-22 production in homeostasis and infection. J Immunol 193, 4602–4613 (2014). [PubMed: 25261485]
59. Choi GB et al. The maternal interleukin-17a pathway in mice promotes autism-like phenotypes in offspring. Science 351, 933–939 (2016). [PubMed: 26822608]
60. Lacy-Hulbert A et al. Ulcerative colitis and autoimmunity induced by loss of myeloid alphav integrins. Proc Natl Acad Sci U S A 104, 15823–15828 (2007). [PubMed: 17895374]
61. Lochner M et al. In vivo equilibrium of proinflammatory IL-17+ and regulatory IL-10+ Foxp3+ RORgamma t+ T cells. J Exp Med 205, 1381–1393 (2008). [PubMed: 18504307]
62. Fan Y et al. Thymus-specific deletion of insulin induces autoimmune diabetes. EMBO J 28, 2812–2824 (2009). [PubMed: 19680229]
63. Archambault AS et al. Cutting edge: Conditional MHC class II expression reveals a limited role for B cell antigen presentation in primary and secondary CD4 T cell responses. J Immunol 191, 545–550 (2013). [PubMed: 23772037]
64. Narni-Mancinelli E et al. Fate mapping analysis of lymphoid cells expressing the NKp46 cell surface receptor. Proc Natl Acad Sci U S A 108, 18324–18329 (2011). [PubMed: 22021440]
65. Schlenner SM et al. Fate mapping reveals separate origins of T cells and myeloid lineages in the thymus. Immunity 32, 426–436 (2010). [PubMed: 20303297]
66. Popmihajlov Z, Xu D, Morgan H, Milligan Z & Smith KA Conditional IL-2 Gene Deletion: Consequences for T Cell Proliferation. Front Immunol 3, 102 (2012). [PubMed: 22590468]
67. Withers DR et al. Cutting edge: lymphoid tissue inducer cells maintain memory CD4 T cells within secondary lymphoid tissue. J Immunol 189, 2094–2098 (2012). [PubMed: 22855716]
68. Kim S et al. CD117(+) CD3(−) CD56(−) OX40Lhigh cells express IL-22 and display an LTi phenotype in human secondary lymphoid tissues. Eur J Immunol 41, 1563–1572 (2011). [PubMed: 21469096]
69. Dutton EE & Withers DR Identification of Murine and Human Innate Lymphoid Cells in Frozen Tissue Sections Using Immunofluorescence. Methods Mol Biol 2121, 51–58 (2020). [PubMed: 32147785]
70. Yang BH et al. Foxp3(+) T cells expressing RORgammat represent a stable regulatory T-cell effector lineage with enhanced suppressive capacity during intestinal inflammation. Mucosal Immunol 9, 444–457 (2016). [PubMed: 26307665]

71. Butler A, Hoffman P, Smibert P, Papalexi E & Satija R Integrating single-cell transcriptomic data across different conditions, technologies, and species. Nat Biotechnol 36, 411–420 (2018). [PubMed: 29608179]

72. Hadley W ggplot2:Elegant Graphics for Data Analysis. (Springer-Verlag New York, 2016).

73. von Mering C et al. STRING: known and predicted protein-protein associations, integrated and transferred across organisms. Nucleic Acids Res 33, D433–437 (2005). [PubMed: 15608232]

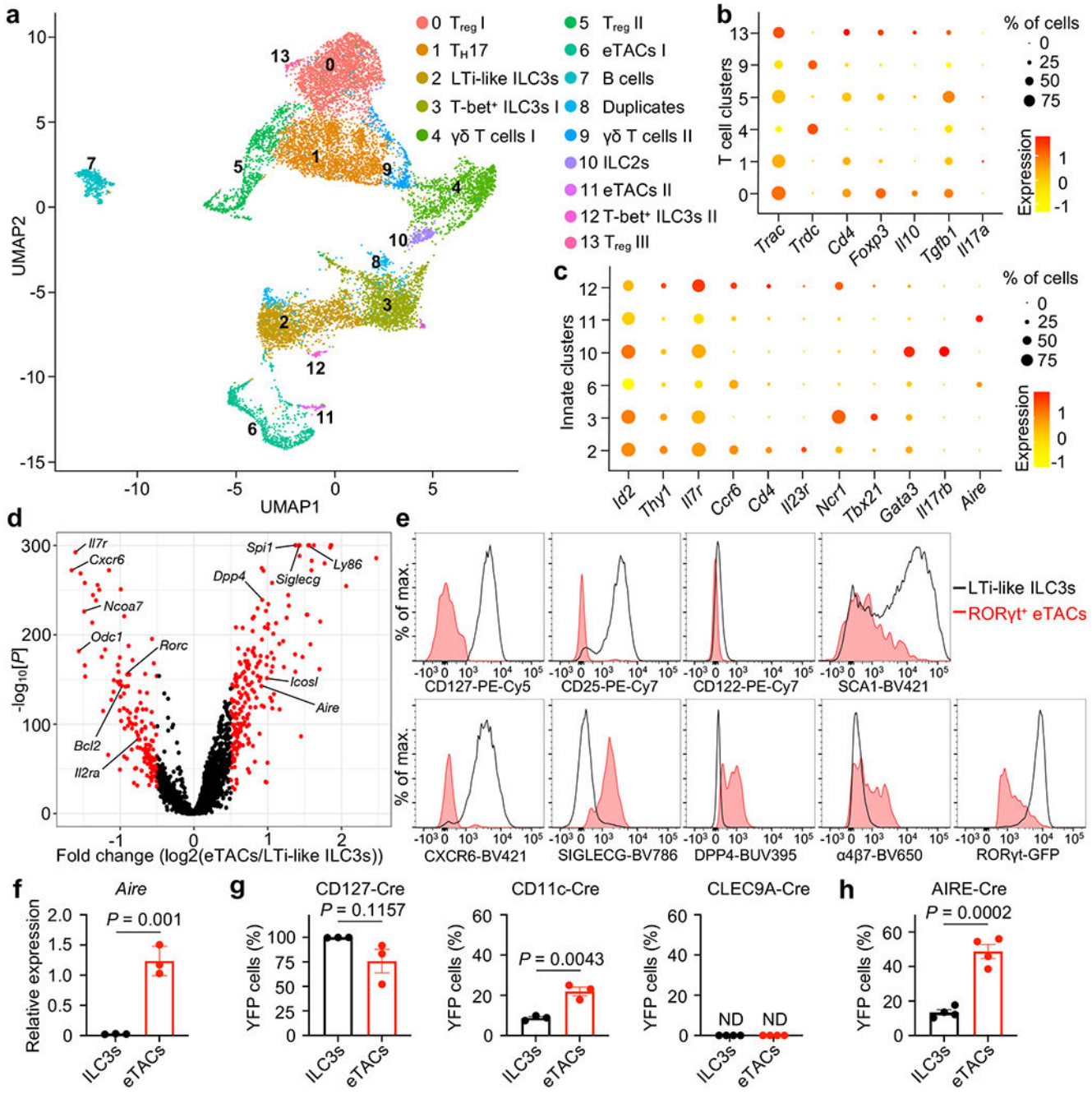

Fig. 1 |. Single-cell resolution of RORγt$^+$ adaptive and innate lymphocytes in the mLN.

a, Uniform manifold approximation and projection (UMAP) of scRNA-seq data from RORγt$^+$ cells in mesenteric lymph node (mLN) from healthy RORγt-eGFP reporter mice. Treg: regulatory T cells; LTi-like ILC3: lymphoid tissue inducer-like group 3 innate lymphoid cells; eTACs: extrathymic Aire-expressing cells; ILC2: group 2 innate lymphoid cells. TCRβ$^+$ GFP$^+$ and TCRβ$^-$ GFP$^+$ cells pooled from 3 mice and 12,948 cells were sequenced. **b**, **c**, Dot plot showing the mean expression (color) of indicated genes in clusters grouped by adaptive lymphocytes (**b**) and innate lymphocytes (**c**), dot size represents the

proportion of cells in a cluster with the gene detected. **d**, Volcano plot of differentially expressed genes between cluster 2 and cluster 6 of scRNA-Seq dataset. **e**, Histogram examination of indicated genes expression in LTi-like ILC3s (black line) and RORγt$^+$ eTACs (red line) from the mLN of RORγt-eGFP reporter mice. **f**, qPCR analysis of *Aire* expression in sort-purified LTi-like ILC3s and RORγt$^+$ eTACs from mLN, relative to *Hprt* (n = 3). **g**,**h**, Frequencies of "fate-mapped" LTi-like ILC3s and RORγt$^+$ eTACs in the mLN of CD127-Cre (n = 3), CD11c-Cre (n = 3), CLEC9A-Cre (n = 4) (**g**) and AIRE-Cre fate-mapping mice (n = 4) (**h**). ND, not detected. Data in **f**-**h** are representative of two or three independent experiments, shown as means ± SEM, statistics shown in **f**, **g**, **h** are obtained by unpaired Student's *t*-test (two-tailed). Statistics in **d** and Supplementary Table 1 were obtained by Wilcoxon test as implemented by Seurat, red dots are significantly different.

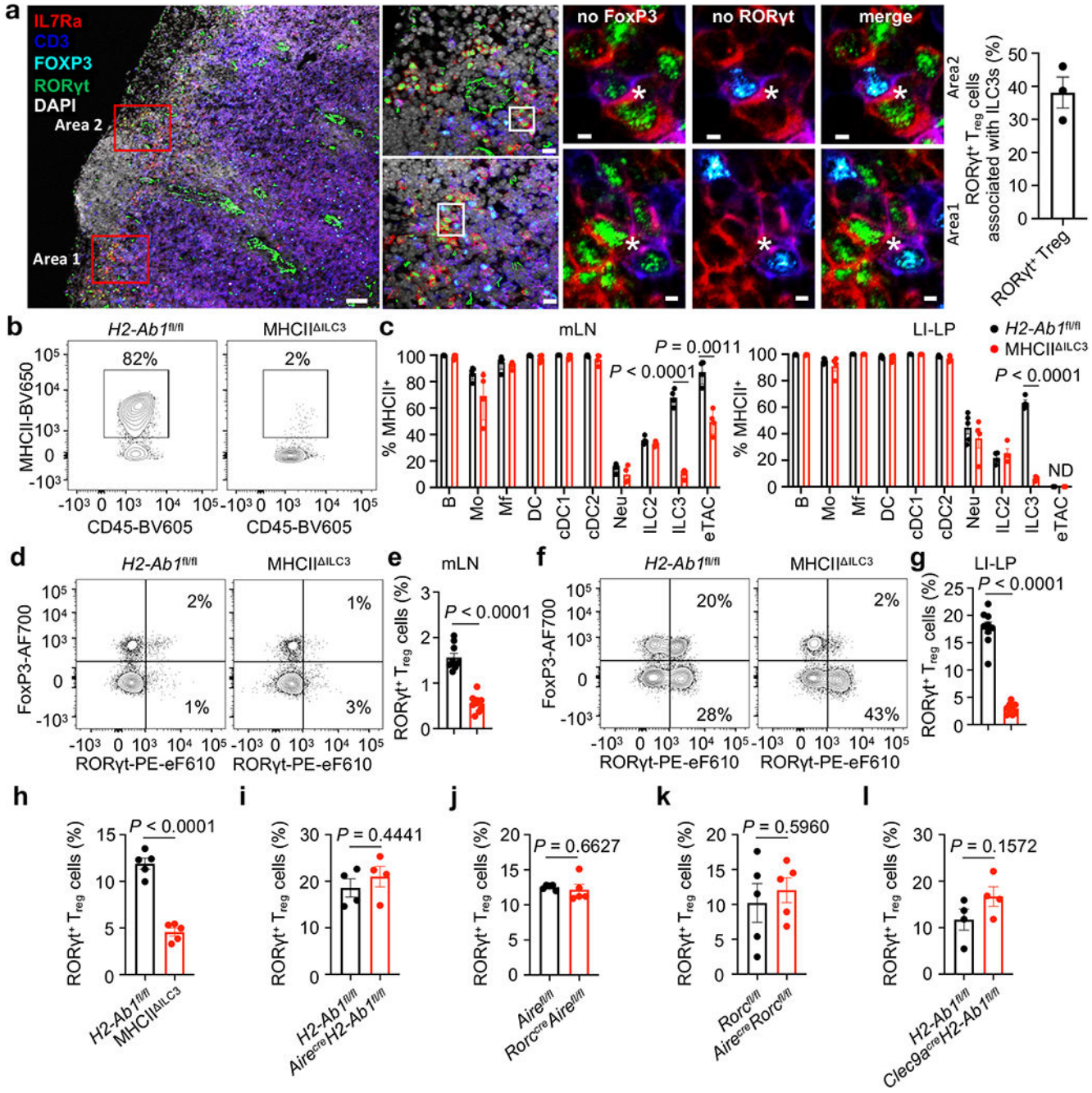

Fig. 2 |. LTi-like ILC3s select for microbiota specific RORγt$^+$ Tregs via MHCII.

a, Left (images), tile-scanned (left) and magnified (column 2) images of mLN, and serial sections (columns 3–5) showing the same interfollicular area as in the left image stained for ILC3s (CD3$^-$IL-7Rα$^+$RORγt$^+$) and RORγt$^+$ Treg cells (CD3$^+$IL$^-$7Rα$^-$FOXP3$^+$RORγt$^+$); the white asterisk indicates the association between ILC3s and RORγt$^+$ Treg cells. Scale bars, 50 μm (left), 10 μm (column 2) and 2 μm (columns 3–5). Right, quantification of the percentage of RORγt$^+$ Treg cells in association with ILC3s in the interfollicular zone (n = 3). **b**, Representative plots of the frequency of MHCII on LTi-like ILC3s in mLN.

c, Quantification of MHCII expression on major MHCII-expressing cells from mLN and LI-LP of *H2-Ab1*$^{fl/fl}$ (n = 5 for B cells (B), monocytes (Mo), macrophages (Mf), dendritic cells (DC), conventional type I and 2 dendritic cells (cDC1 and cDC2) and neutrophils (Neu); n = 4 for ILC2, ILC3 and eTACs) and MHCII$^{\Delta ILC3}$ mice (n = 4). **d**-**g**, Representative flow cytometry plot of the frequency (% of CD4^{+} T cells) (**d**, **f**) and quantification (**e**, **g**) of RORγt^{+} Tregs in mLN and LI-LP of *H2-Ab1*$^{fl/fl}$ and MHCII$^{\Delta ILC3}$ mice (n = 9). **h**-**l**, Quantification of RORγt^{+} Tregs (% of Tregs) in mLN of MHCII$^{\Delta ILC3}$ mice (n = 5) (**h**), *Aire*^{Cre}*H2-Ab1*$^{fl/fl}$ mice (n = 4) (**i**), *Rorc*^{Cre}*Aire*$^{fl/fl}$ mice (n = 5) (**j**), *Aire*^{Cre}*Rorc*$^{fl/fl}$ mice (n = 5) (**k**) and *Clec9a*^{Cre}*H2-Ab1*$^{fl/fl}$ mice (n = 4) (**l**) relative to littermate control mice. Data in **d**-**g** are pooled from two independent experiments. Data in **h**-**l** are representative of two independent experiments. Data are shown as mean ± SEM, statistics shown in **c** are obtained by multiple unpaired *t*-test (two-tailed), statistics shown in **e**, **g**, **h**-**l** are obtained by unpaired Student's *t*-test (two-tailed).

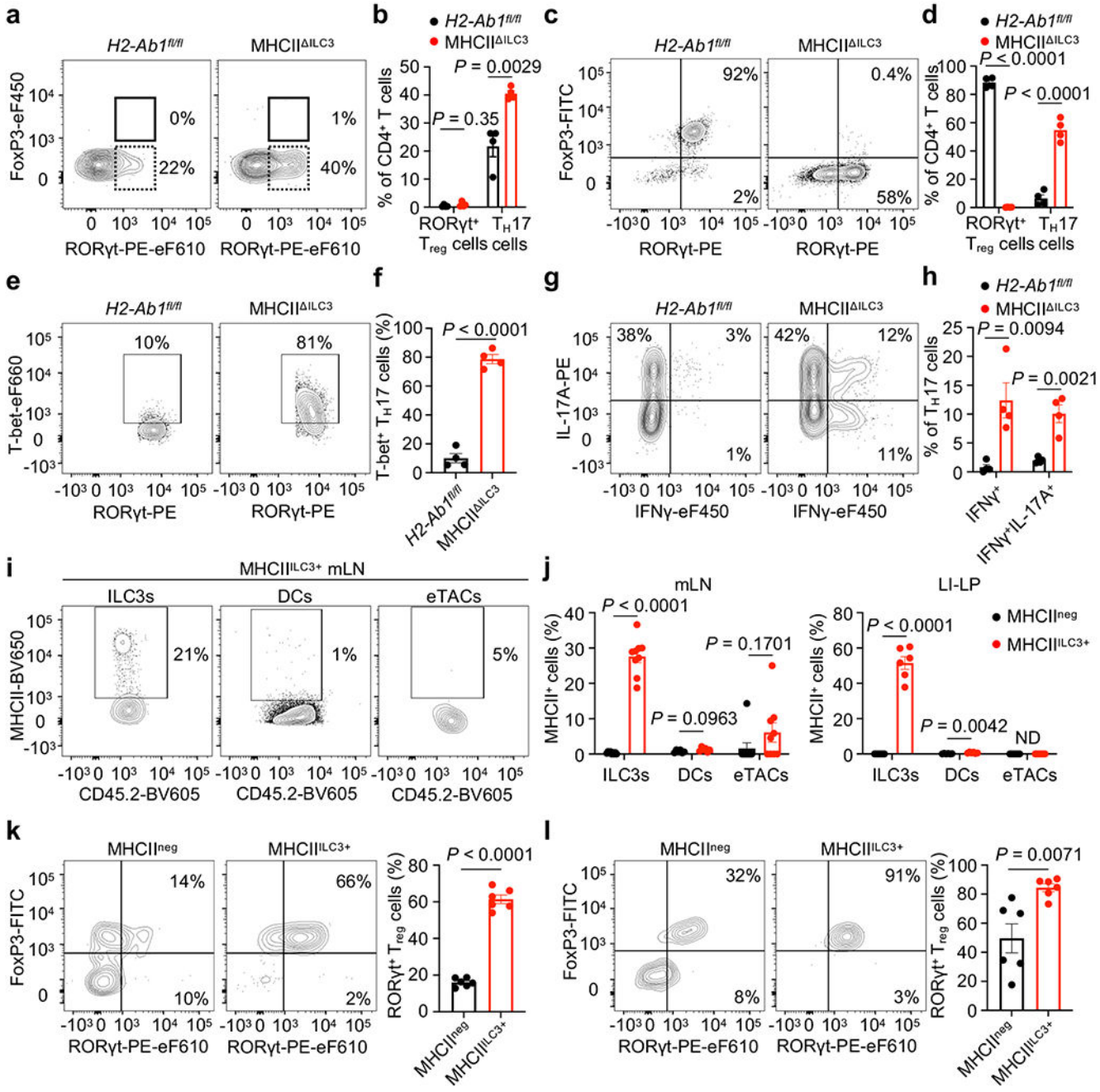

Fig. 3 |. MHCII$^+$ ILC3s are sufficient for selection of microbiota specific RORγt$^+$ Tregs.

a–d, Flow cytometry plots (**a,c**) and frequencies (**b,d**) of RORγt$^+$ Tregs (RORγt$^+$FOXP3$^+$) and Th17 cells (RORγt$^+$FOXP3$^-$) in Peyer's patch for SFB-specific (CD45.1$^-$CD90.1$^+$CD4$^+$ T cells; **a,b**) and in LI-LP for H. hepaticus-specific (CD45.1$^+$CD90.1$^-$CD4$^+$ T cells; **c,d**) from *H2-Ab1*$^{fl/fl}$ and MHCIIΔILC3 mice (n = 4). **e**, **f**, Representative flow cytometry plots of the frequency (T-bet$^+$ among *H. hepaticus*-specific RORγt$^+$FoxP3$^-$ Th17 cells) (**e**) and quantification (**f**) of T-bet$^+$ *H. hepaticus*-specific Th17 in LI-LP of *H2-Ab1*$^{fl/fl}$ and MHCII$^{\Delta ILC3}$ mice as shown in (**c**) (n = 4). **g**, **h**, Representative

flow cytometry plots of the frequency (IL-17A$^+$ and/or IFNγ^+ cells among *H. hepaticus*-specific RORγt$^+$FoxP3$^-$ Th17 cells) (**g**) and quantification (**h**) of IFNγ^+ and IFNγ^+IL-17A$^+$ cells among *H. hepaticus*-specific Th17 in LI-LP of *H2-Ab1*$^{fl/fl}$ and MHCII$^{\Delta ILC3}$ mice as shown in (**c**) (n = 4). **i**, **j**, Representative flow cytometry plots of the frequency (**i**) and quantification (**j**) of MHCII expression on ILC3s, DCs and eTACs (gated as CD127$^-$CD90$^-$) in mLN and LI-LP of MHCII^{neg} and MHCII^{ILC3+} mice (n = 6 or 9). ND, not detected. **k**, **l**, Representative flow cytometry plots of the frequency and quantification of RORγt$^+$ Tregs (RORγt$^+$FoxP3$^+$ among *H. hepaticus*-specific CD4$^+$ T cells) were analyzed for transgenic T cells in mLN (**k**) and LI-LP (**l**) of MHCII^{neg} and MHCII^{ILC3+} mice (n = 6). Data in **a**-**h** are representative of two independent experiments. Data in **i**-**l** are pooled from two or three independent experiments. Data are shown as mean ± SEM, statistics are obtained by unpaired Student's *t*-test (two-tailed).

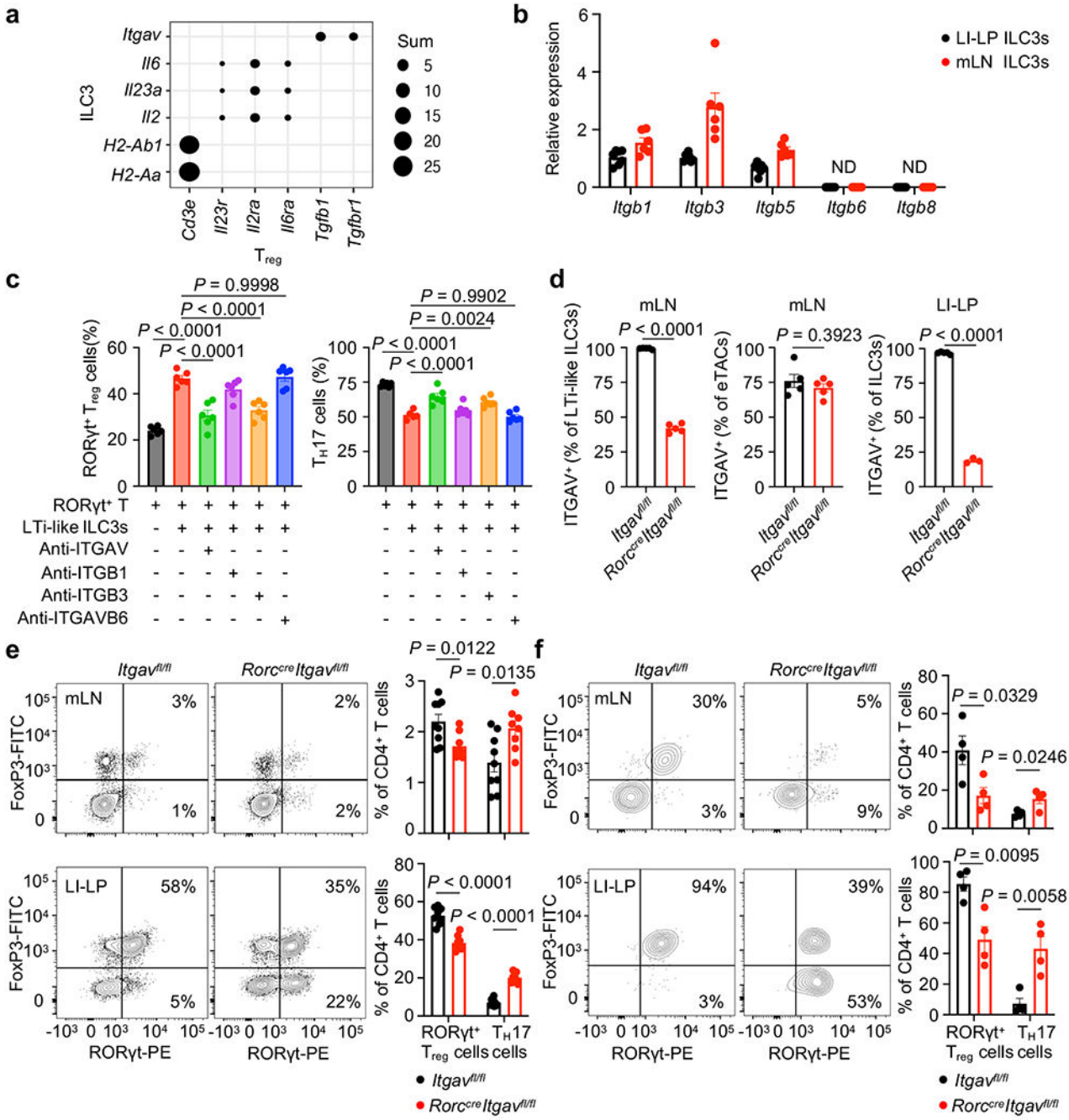

Fig. 4 |. Itgav on LTi-like ILC3s promotes RORγt$^+$ Treg homeostasis.

a, Dot plot showing selected genes expressed in ILC3 (*y* axis) and Treg (*x* axis) cell clusters. **b**, qPCR analysis of *Itgb1, Itgb3, Itgb5, Itgb6 and Itgb8* expression in sort-purified LTi-like ILC3s from LI-LP (n = 7) and mLN (n = 6), relative to *Hprt*. ND, not detected. **c**, Sort-purified RORγt$^+$CD4$^+$ T cells and LTi-like ILC3s from LI-LP and mLN (n = 12, each dot represents samples pooled from 2 mice) were co-cultured for 72 hours under indicated conditions, and frequencies of RORγt$^+$ Tregs and Th17 cells were analyzed by flow cytometry. **d**, Quantification of Itgav on LTi-like ILC3s and eTACs in mLN (n = 5),

and quantification of Itgav on ILC3s in LI-LP of *Itgav*$^{fl/fl}$ and *Rorc*^{Cre}*Itgav*$^{fl/fl}$ mice (n = 5 or 3 per group). **e**, Representative flow cytometry plot of the frequency (% in CD4$^+$ T cells) (left panel) and quantification (right panel) of RORγt$^+$ Tregs and Th17 cells in mLN (top panel) and LI-LP (bottom panel) of *Itgav*$^{fl/fl}$ (n = 9) and *Rorc*^{Cre}*Itgav*$^{fl/fl}$ mice (n = 8). **f**, Representative flow cytometry plot of the frequency (left panel) and quantification (right panel) of RORγt$^+$ Tregs (RORγt$^+$FoxP3$^+$ among *H. hepaticus*-specific CD4$^+$ T cells) and Th17 cells (RORγt$^+$FoxP3$^-$ among *H. hepaticus*-specific CD4$^+$ T cells) were analyzed in mLN (top panel) and LI-LP (bottom panel) of *Itgav*$^{fl/fl}$ and *Rorc*^{Cre}*Itgav*$^{fl/fl}$ mice (n = 4). Data in **d**, **f** are representative of two independent experiments. Data in **c**, **e** are pooled from two independent experiments. Data are shown as means ± SEM, statistics shown in **c** are obtained by one-way ANOVA with Tukey's multiple comparisons test, statistics shown in **d**-**f** are obtained by unpaired Student's *t*-test (two-tailed).

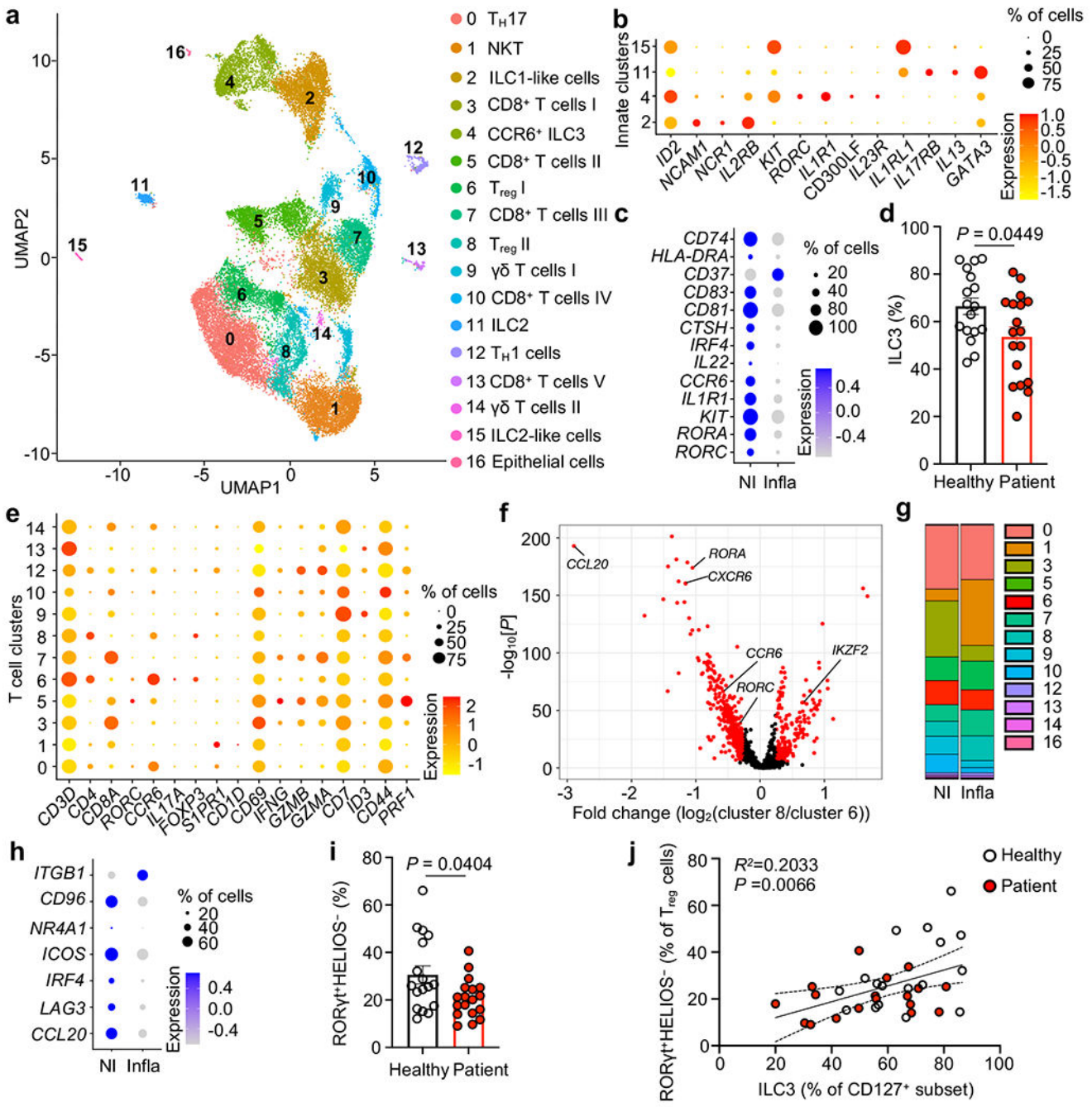

Fig. 5 |. Interactions between ILC3 and RORγt^{+} Treg are altered in human IBD.

a, UMAP plots of scRNA-seq data on ILCs and T lymphocytes from the inflamed and non-inflamed intestine in human IBD. **b**, Dot plot showing the mean expression (color) of indicated genes in clusters grouped by low *CD3E* expression, dot size represents the proportion of cells in a cluster with the gene detected. **c**, A dot plot showing the mean expression (colour) of indicated genes in cluster 4 as indicated in (**a**) in non-inflamed (NI) versus inflamed tissue (Infla). **d**, Quantification of ILC3 frequency in a cohort of IBD patients. Healthy donor n = 17, IBD patient n = 18. **e**, Dot plot showing the mean expression

(color) of indicated genes in clusters grouped by high *CD3E* expression. **f**, Volcano plot of differentially expressed genes between cluster 6 and cluster 8 as indicated in (**a**). **g**, Bar graph showing the composition of T lymphocytes as indicated in (**a**). **h**, Expression of indicated genes in cluster 6 in non-inflamed versus inflamed tissue as indicated in (**a**). **i**, Quantification of frequency of RORγt$^+$ Tregs among total Tregs in a cohort of IBD patients as indicated in (**d**). **j**, Correlation analyses between the ILC3 and RORγt$^+$ Treg frequencies as indicated in (**d, i**). Data in **d**, **i** are shown as means ± SEM, statistics shown in **d**, **i** are performed using Mann–Whitney *U*-test (unpaired), correlative analyses in **j** are compared by Pearson's rank correlation coefficient (R^2). Statistics are calculated by two-tailed test. Statistics in **f** and Supplementary Table 2 were obtained by Wilcoxon test as implemented by Seurat, red dots are significantly different.